Technical Reports

CENTRO EURO-MEDITERRANEO
PER I CAMBIAMENTI CLIMATICI

ISC – Impact on Soil and Coasts

Data about rainfall-induced landslides in pyroclastic soils: the cases of Camaldoli hill, Naples and of Nocera Inferiore

prof. Luciano Picarelli
Analisi e Monitoraggio del Rischio Ambientale, AMRA

prof. Filippo Vinale
Analisi e Monitoraggio del Rischio Ambientale, AMRA

Centro Euro-Mediterraneo
per i Cambiamenti Climatici
www.cmcc.it

February 2008 ■ TR

Data about rainfall-induced landslides in pyroclastic soils: the cases of Camaldoli hill, Naples and of Nocera Inferiore

Summary
The report illustrates rainfall, geomorphological and geotechnical data regarding landslides occurred in pyroclastic soils.
The first case concerns an area located in the western sector of the urban district of Naples, known as Camaldoli hill (landslides occurred on October 13th, 2004, and on September 17th, 2005). The second case regards the northern slope of Monte Sant'Angelo di Cava mountain, located in the Nocera Inferiore town (March, 4th, 2005).

Keywords: rainfall-induced landslides, monitoring, pyroclastic soils

JEL Classification:

Address for correspondence:

prof. Luciano Picarelli
E-mail: luciano.picarelli@amracenter.com

prof. Filippo Vinale
E-mail: filippo.vinale@amracenter.com

A.M.R.A. S.c.a.r.l.
Via Nuova Agnano, 11
80125 Napoli, Italy

CONTENTS

1. Foreword

During the last decades, several rainfall-induced landslides occurred in Campania Region (Southern Italy), mobilizing terrains whose origin is associated with past volcanic activity (pyroclastic deposits). These landslides, which may be classified as extremely rapid and shallow flowslides and debris flows (Hungr et al., 2001), caused hundreds victims and huge economical damages to property.
The cases examined in this report regard an area set inside the western sector of the urban district of Naples, known as Camaldoli hill, and the northern slope of Monte Sant'Angelo di Cava mountain, located in the Nocera Inferiore town.
While the events that affected the Camaldoli hill (recorded on October, 13th, 2004 and on September 17th, 2005) didn't provoke heavy damages, the Nocera flowslide (March, 4th, 2005) killed three people, whose house was destroyed by the impact induced by the soil mass.

This report provides data about the geomorphological setting, properties of involved soils and monitoring. All data will be used in analyses which will be carried out for the validation of a numerical model for prediction of rainfall-induced landslides over vast areas.

2. The case of Camaldoli hill

The Camaldoli hill, set in the western sector of the urban area of Naples, represents the highest peak (458 m a.s.l.) of a still active volcanic district, known as Phlegraean Fields (Fig. 2.1). This district is the result of two main collapses related to the Campanian Ignimbrite and Neapolitan Yellow Tuff eruptions, which respectively happened 39.000 and 12.000 years ago.
The hill, whose name is due to the Hermitage placed at its top, is structurally characterized by two main fronts (Fig. 2.2): the first one is oriented to West toward the urbanized district of Pianura, while the second one is oriented to the South-East toward the urbanized district of Soccavo.
The hillslopes, about 200 m high and characterized by high angles, are stepped because of the alternance of rocks (jointed weak tuffs) and soils (pyroclastic deposits), both having a volcanic origin.

Figure 2.1. Geographic location of the Camaldoli hill (Calcaterra et al., 2003)

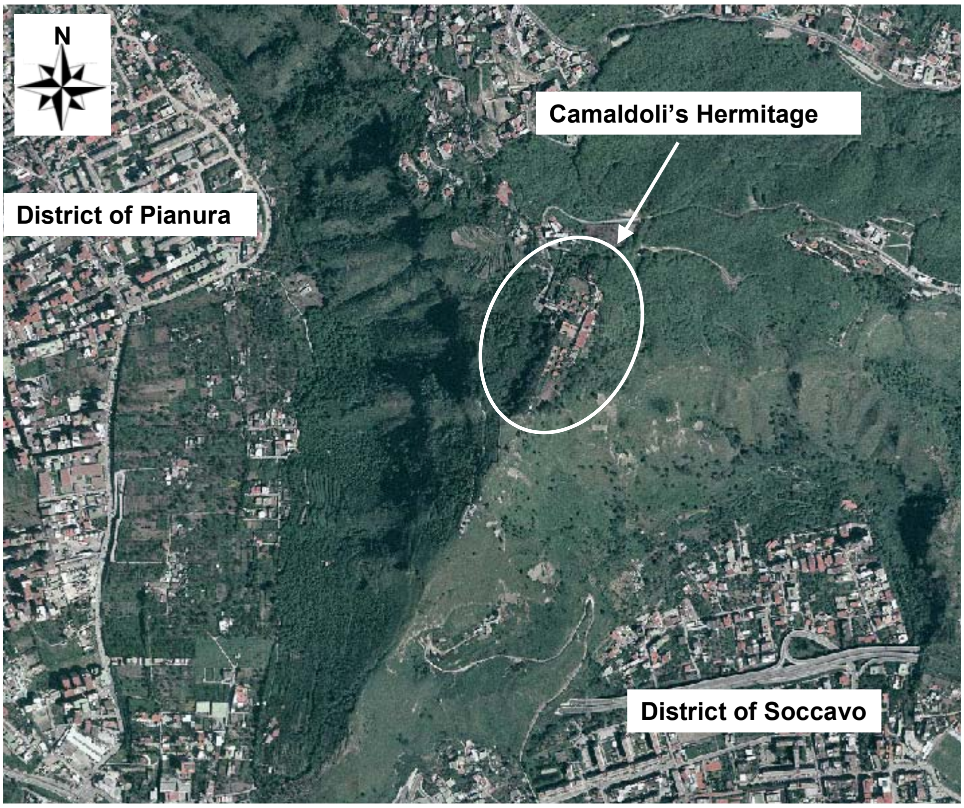

Figure 2.2. Aerial view of the Camaldoli hill

2.1 Geological and geomorphological setting

The Camaldoli hill is placed inside a 2.000 Km^2 wide region set to North of Naples, named Campanian Plain (Fig. 2.3), which represents a faulted depression created by the regional subsidence of a carbonate basement along a NE–SW oriented fault system. Its features are therefore the result of extensional tectonic processes caused during the Pliocene-Quaternary by opening of Tyrrhenian basin and Europe-Africa compression, which induced the deepening of the surrounding Apennine region and the formation of widespread graben-like structures along the Tyrrhenian border of the chain.
The Campanian Plain has been affected by an intense volcanic activity for at least 600.000 years: for this reason, it has been also called Campanian Volcanic Zone. About 39.000 years ago, the violent explosive eruption of Campanian Ignimbrite generated very large volumes (about 150 km^3) of pyroclasts deposits, which filled the graben. Those volumes were so huge that caused the definitive aggrading of the sedimentary basement of the Plain. A successive violent eruption occurred 12.000 years ago and produced the Neapolitan Yellow Tuff.

Every pyroclastic deposit of the Campanian Region took origin by the activity of two main volcanic settings of the Campanian Volcanic Zone: the Somma-Vesuvius district and the Phlegraean Fields (Fig. 2.1). The Somma-Vesuvius district corresponds to large sectors of the Campanian Apennine chain, which include the Sorrento Peninsula, the Lattari Mts., the Sarno Mts., the Avella Mts. and the Caserta Mts.. This setting is characterized by a Mesozoic carbonate bedrock covered by thin sequences of pyroclastic products (generally lower than 5 m). On the other hand, the Phlegraean Fields include Naples and the islands of Ischia and Procida. That district consists of a well defined subsiding caldera (Fig. 2.4) constituted by more than 25 volcanic edifices, which essentially developed after the Neapolitan Yellow Tuff eruption. Its activity has been characterized by alternating periods of quiescence and of intense volcanism, which was also responsible of repeated sea level variations, until September 1538, when the last eruption took place. The bedrock is made up of Late Pleistocene volcanic tuffs and lavas and is mantled by loose pyroclastic terrains, whose thickness can attain some ten of metres.

The pyroclastic deposits outcropping in the Neapolitan area present significant local differences. In particular, they display both lithified and unlithified facies related to eruptive and emplacement conditions, which significantly affect their behaviour. As reported in Figure 2.5, the pyroclastic materials outcropping in the town of Naples can be classified as:
1) unlithified Neapolitan Yellow Tuff, or Pozzolana (YTP);
2) lithified Neapolitan Yellow Tuff (NYT);
3) pyroclastic products of the volcanic activity of Phlegraean Fields younger than 15 ky (Intracaldera Phlegraean pyroclastic Deposits, IPD).

Figure 2.5 shows the outcrops of Neapolitan Yellow Tuff in distal and proximal areas with a clear interface between lithified and unlithified zones throughout the city. In particular, IPD consist of a complex sequence of eruptive products as ashes, lapilli, scoriae and pumices which crop out above the Neapolitan Yellow Tuff formation. Those

terrains are typical of the Camaldoli hill, which occupies the north-eastern margin of the Phlegraean Fields (Fig. 2.5).
The Camaldoli hill includes the remnants of two partially superposed tuff cones, lying between Campanian Ignimbrite and Neapolitan Yellow Tuff, which in turn are mantled by a sequence of loose pyroclastic, anthropic and epiclastic deposits, characterized by sudden thickness variations. The surficial portion (50-100 cm) has been weathered by atmospheric agents and anthropic and biological activity. In particular, going from the most ancient to the youngest deposits, the area presents (Fig. 2.6):

- the lithified formation called Torre Franco tuff, which was deposited before the Campanian Ignimbrite explosion (>39.000 years ago);
- the lithified formations known as Piperno and Breccia Museo, deposited during the Campanian Ignimbrite explosion (39.000 years ago);
- Intracaldera Phlegraean pyroclastic deposits formed before the Neapolitan Yellow Tuff explosion (>12.000 years ago);
- the lithified Neapolitan Yellow Tuff (12.000 years ago);
- Intracaldera Phlegraean pyroclastic deposits formed after the Neapolitan Yellow Tuff explosion (<12.000 and <10.000 years ago);
- artificial deposits (anthropic and mine products)

From a structural point of view, the actual setting of the Camaldoli hill is the result of slope failures and deformational processes associated with:

- volcanotectonism;
- faults activation (the hill is affected by three fault systems);
- water action;
- landslides.

The hillslopes are about 200 m high and present high angles upslope (some of them are almost vertical) and low angles downslope, ranging in the interval 0°-15° next to the urbanized area (Fig. 2.7). The slopes are crossed by many channels, whose profiles are longitudinally stepped because of the alternance of rocks (lithified tuffs) and soils (loose pyroclastic deposits). The latter deposits are generally weathered in their upper layers, as a consequence of interaction with decay agents and of past slope failures.
Landslides that have affected Camaldoli hill, have been induced by rainfall events involving as tuff as pyroclastic soils (Fig. 2.8). The upper rock formations have been involved in “falls” and “falls/avalanches” mobilizing up to some tens of cubic metres. Some landslides reach the lowest sectors of the slope, very close to the urbanized area. On the other hand, the landslides occurring in pyroclastic soils are generally very shallow (maximum depth around 2 m), and show typical features of “slides” or of mixed “slides/flows”: such events usually start as slides in the upper portion of the hill and evolve in flows along channels. As can be also seen in Figure 2.8, the hillslopes most frequently subjected to landslides are those exposed along the south-eastern side of the hill. That front was also interested by the landslides that were activated on October, 13th, 2004 and September, 17th, 2005: some information about these two events are reported in the next section.

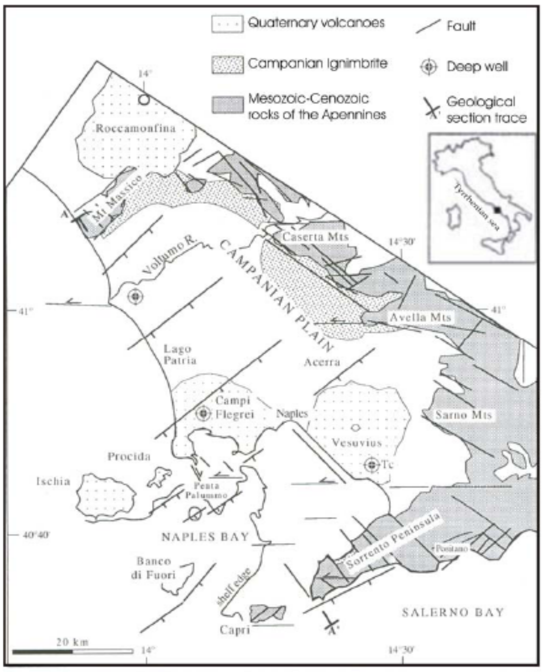

Figure 2.3. Southern sector of the Campanian Plain

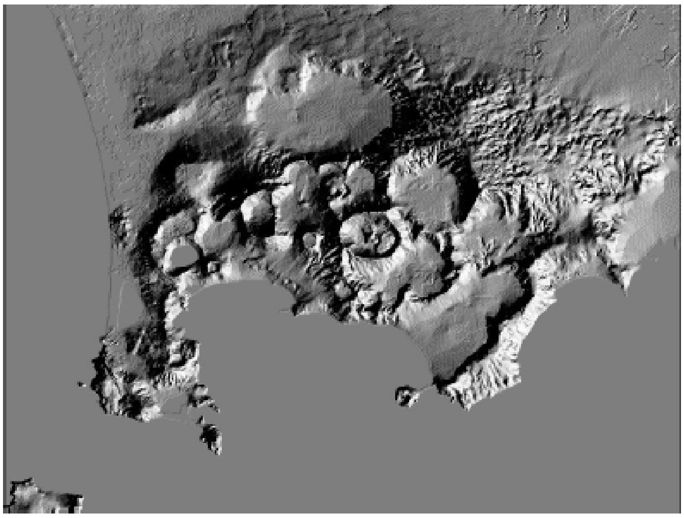

Figure 2.4. The Phlegraean Fields volcanic district

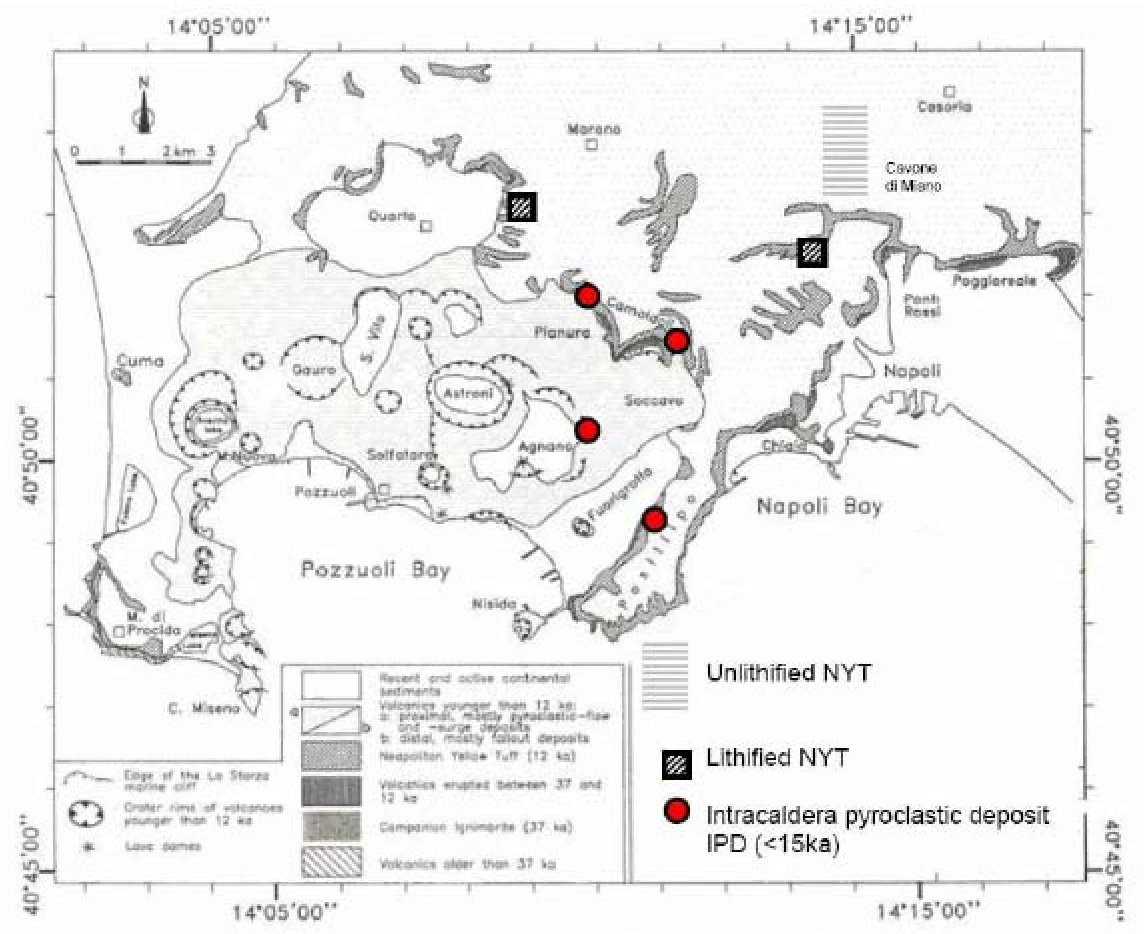

Figure 2.5. Geological map of the Phlegraean Fields

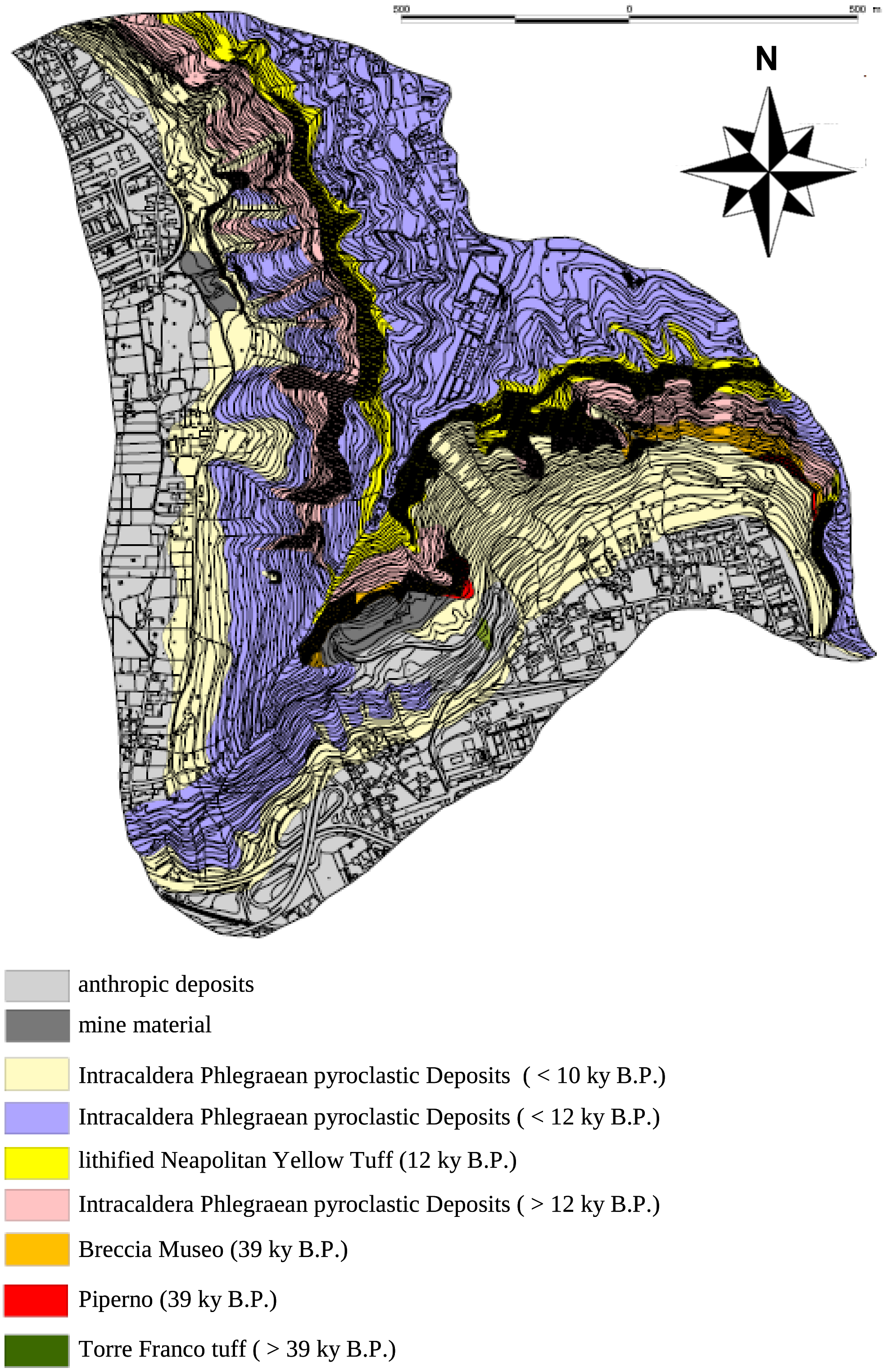

Figure 2.6. Geological map of the Camaldoli hill (modified from Di Crescenzo et al., 2007)

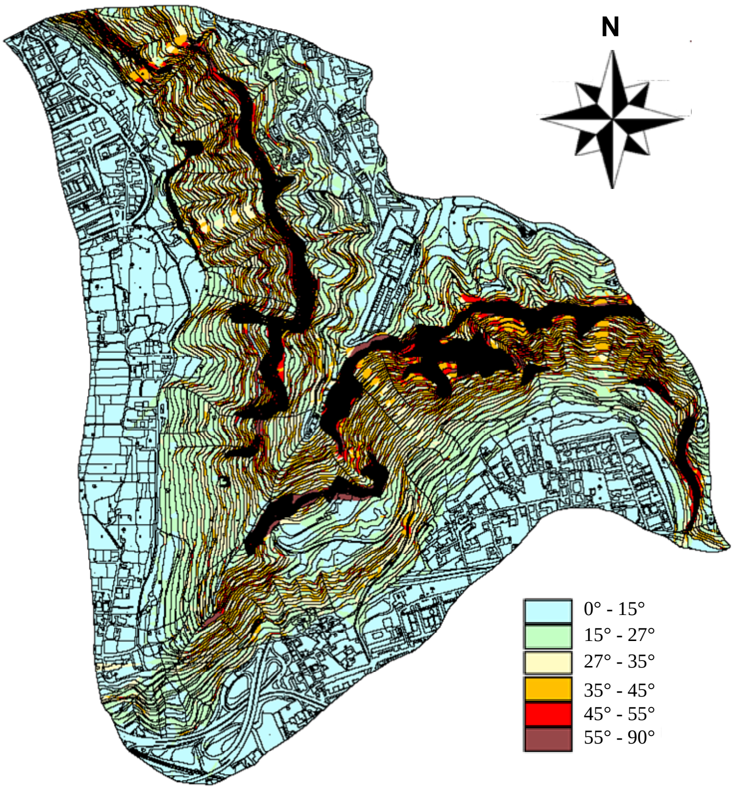

Figure 2.7. Topographic slope map of the Camaldoli hill (modified from Di Crescenzo et al., 2007)

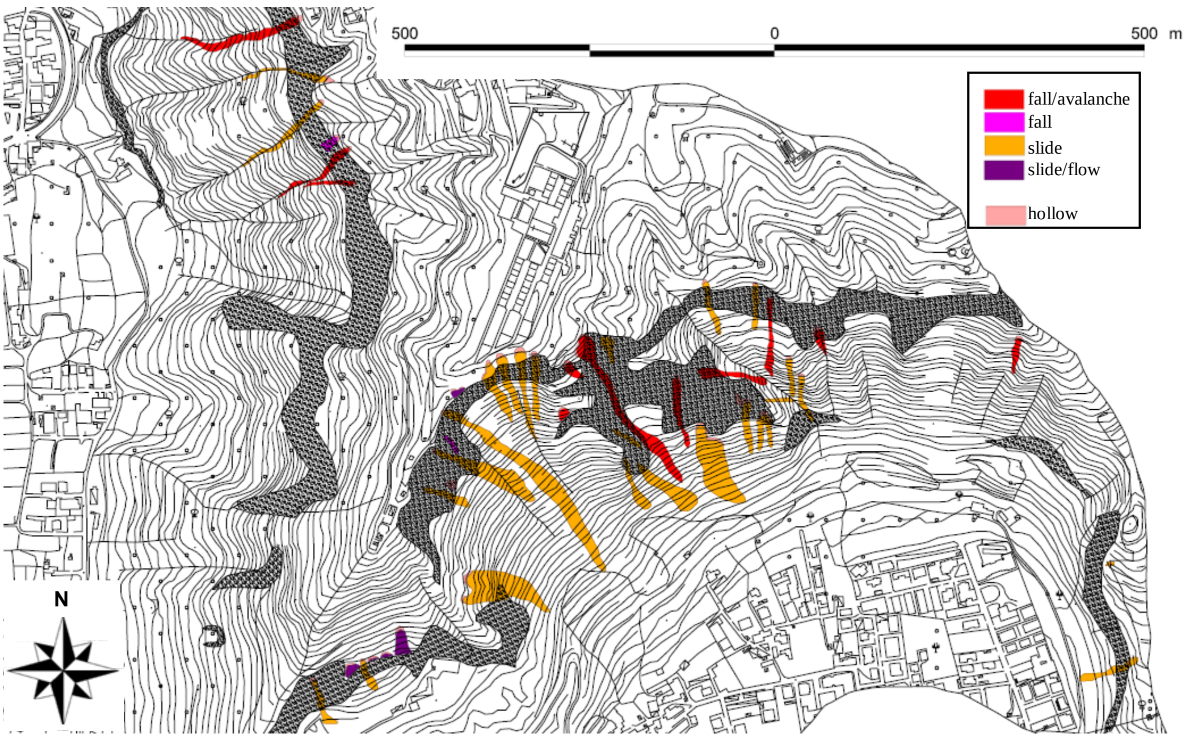

Figure 2.8. Landslides occurred between 1997 and 2007 (modified from Di Crescenzo et al., 2007)

2.2 Examined test cases

2.2.1 Test case nr. 1: October, 2004

On October 13th, 2004, two landslides were activated along the south-eastern side of the Camaldoli hill. These landslides, classifiable as “slides”, have been identified as A and B in the Figure 2.9: they presented a thickness ranging between 0.5 m and 2.0 m and average width and length respectively equal to 10 m and 85 m. While the slide A involved the Intracaldera Phlegraean pyroclastic deposits, and the younger IPD set downslope, the slide B directly originated within these last terrains.

a)

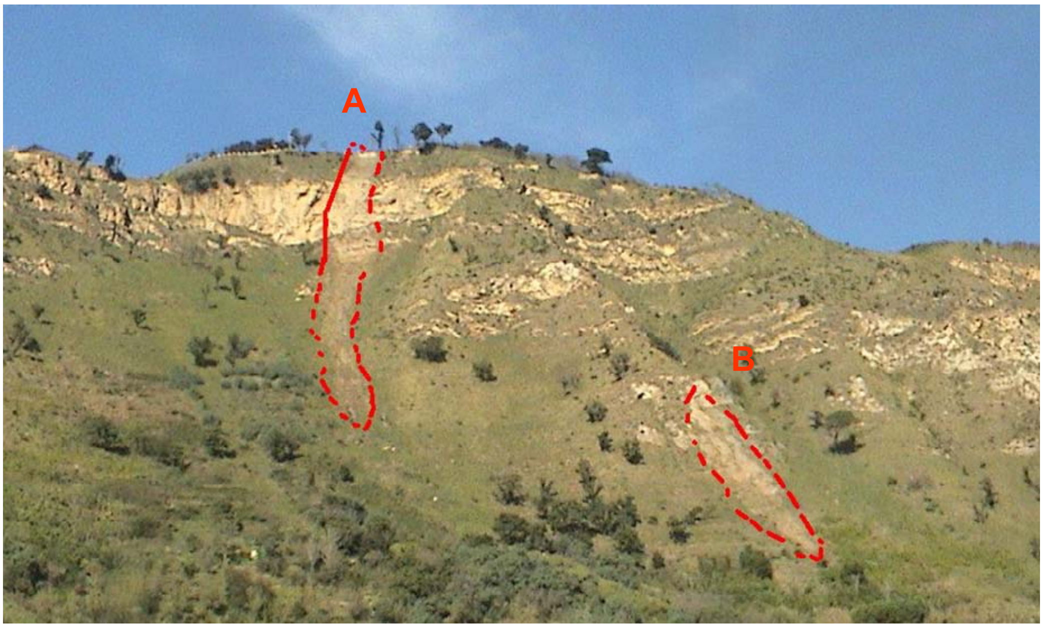

b)

Figure 2.9. Landslides occurred on October 13th, 2004

Rainfall heights have been measured a pluviometer, set by the Civil Protection Agency of the Campania Region near to the Hermitage at an altitude of 384 m a.s.l. Available data (with a hourly frequency) cover the period October 18th, 2000 - December 31st, 2007. Comparing all data (Fig. 2.10), the daily rainfall cumulated on October 13th, 2004 (47.6 mm) is the 10th highest, having been previously overcome only 5 times (on May 5th, 2001; September 15th, 2001; August 29th, 2002; September 9th, 2003; October 18th, 2003) and 4 times later on (March 4th, 2005; September 17th, 2005; September 22nd, 2005; November 6th, 2005). In particular, the rainfallconcentrated during a rather short time interval (7 hours) distributed between 16:00 and 23:00 (Fig. 2.11): the hourly peak (19.2 mm) was registered between 18:00 and 19:00.
Unfortunately, the exact time of landslide triggering is unknown.

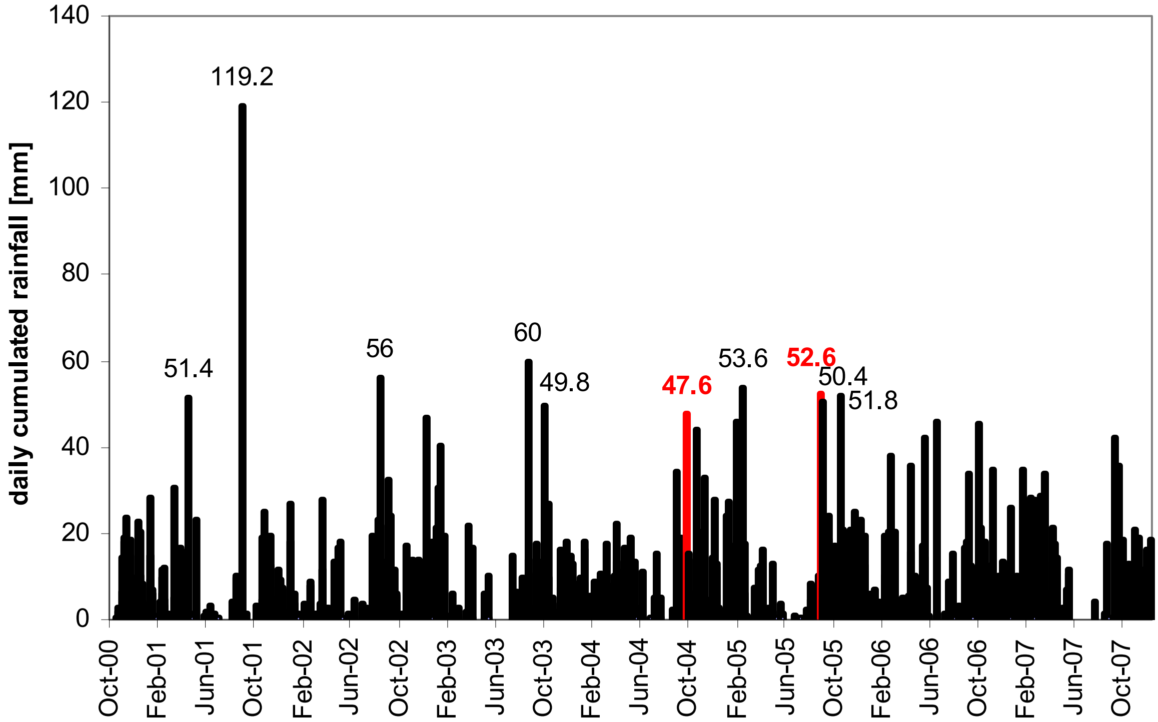

Figure 2.10. Daily cumulated rainfall measured during the period 18/10/2000 – 31/12/2007: red lines represent the data concerning October, 13, 2004 (47.6 mm) and September 17, 2005 (52.6 mm)

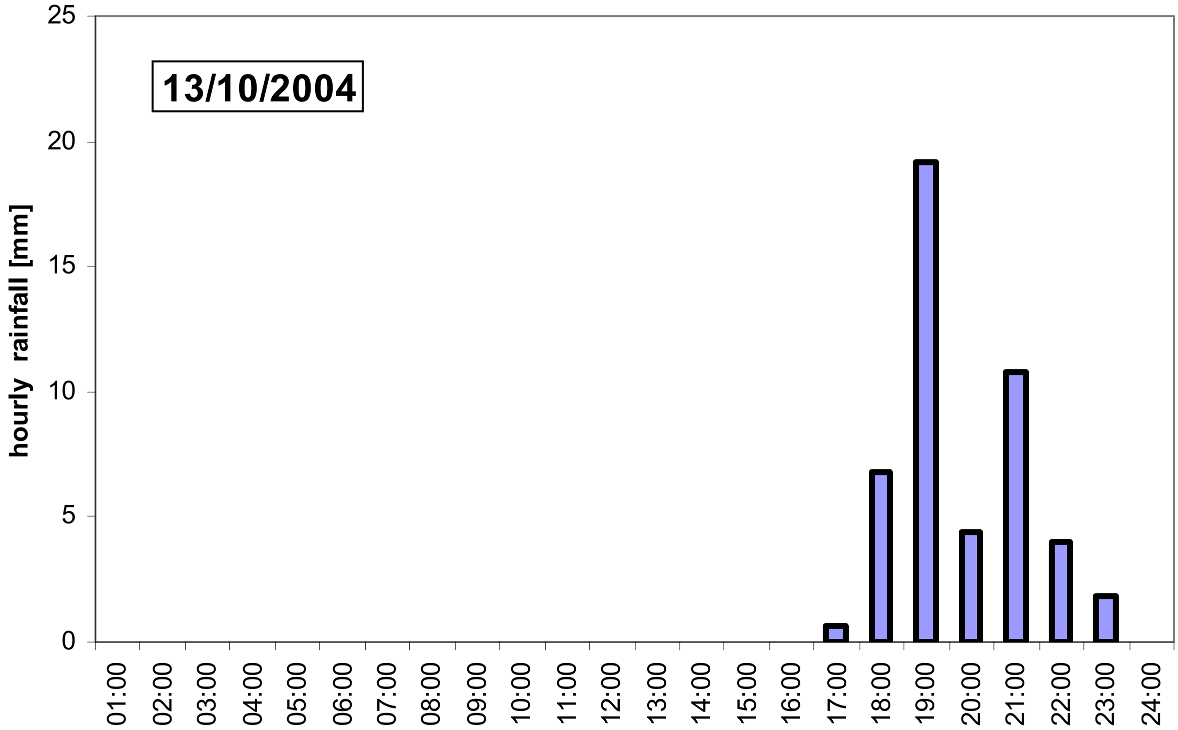

Figure 2.11. Hourly rainfall measured on October 13th, 2004

2.2.2 Test case nr. 2: September, 2005

During the night between September 17th and 18th, 2005, three shallow "slides" (named C, D and E in Figure 2.12) were triggered at the foot of the Hermitage, in the Intracaldera Phlegraean pyroclastic deposits, by one of the most intense rainfall events registered by the pluviometer. In particular, the hourly peak measured between 23:00 and 24:00 (44.2 mm) (Fig. 2.13) has been overcome only two times (62.8 mm on September 15th, 2001, and 47.0 mm on August 29th, 2002), while, as reported in Figure 2.10, the daily cumulated rainfall measured on September 17th, 2005 (52.6 mm) has been overcome only 4 times (119.2 mm on September 15th, 2001; 56.0 mm on August 29th, 2002; 60.0 mm on September 9th, 2003; 53.6 mm on March 4th, 2005).
The rainfall event lasted 7 hours. No information is available about the time of landslides triggering.

Having both the landslides events involved the Intracaldera Phlegraean pyroclastic deposits, next section will report some information about their geotechnical properties.

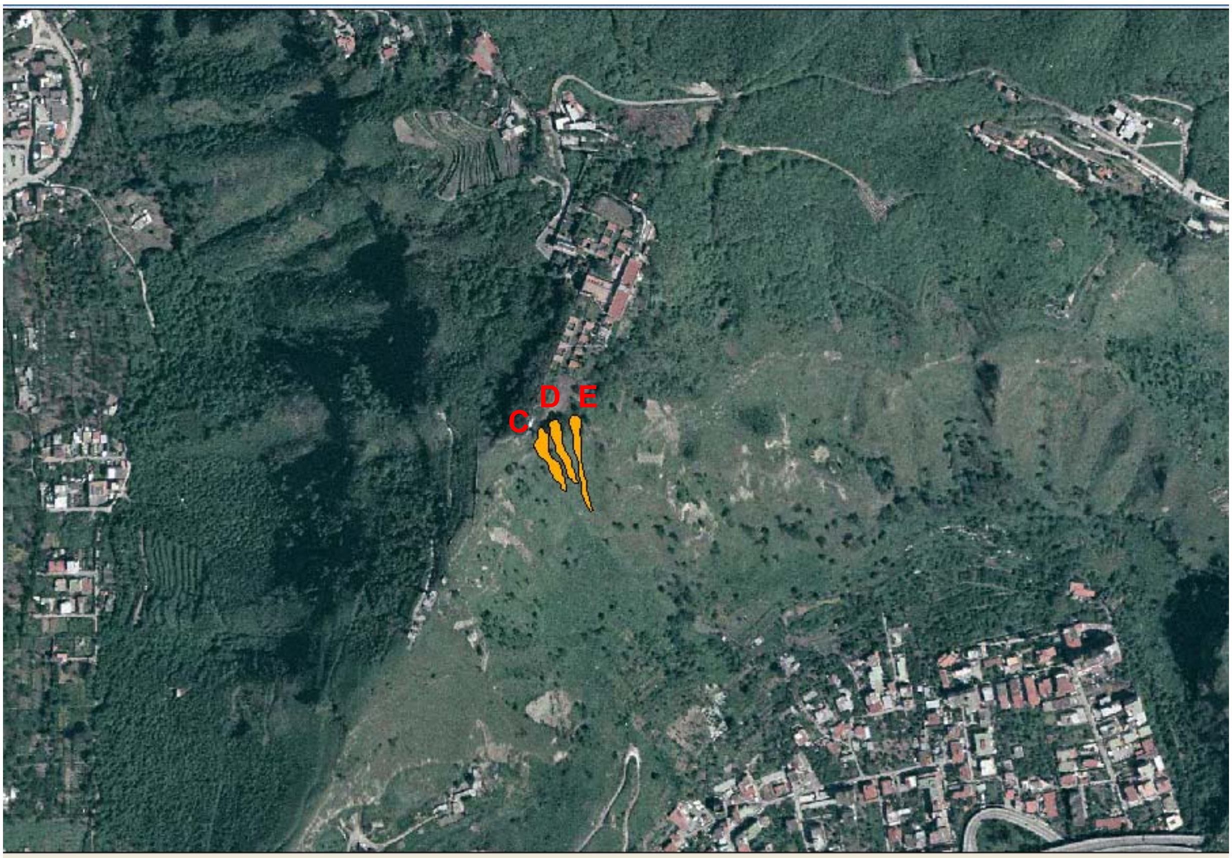

Figure 2.12. Landslides occurred on September 17th, 2005

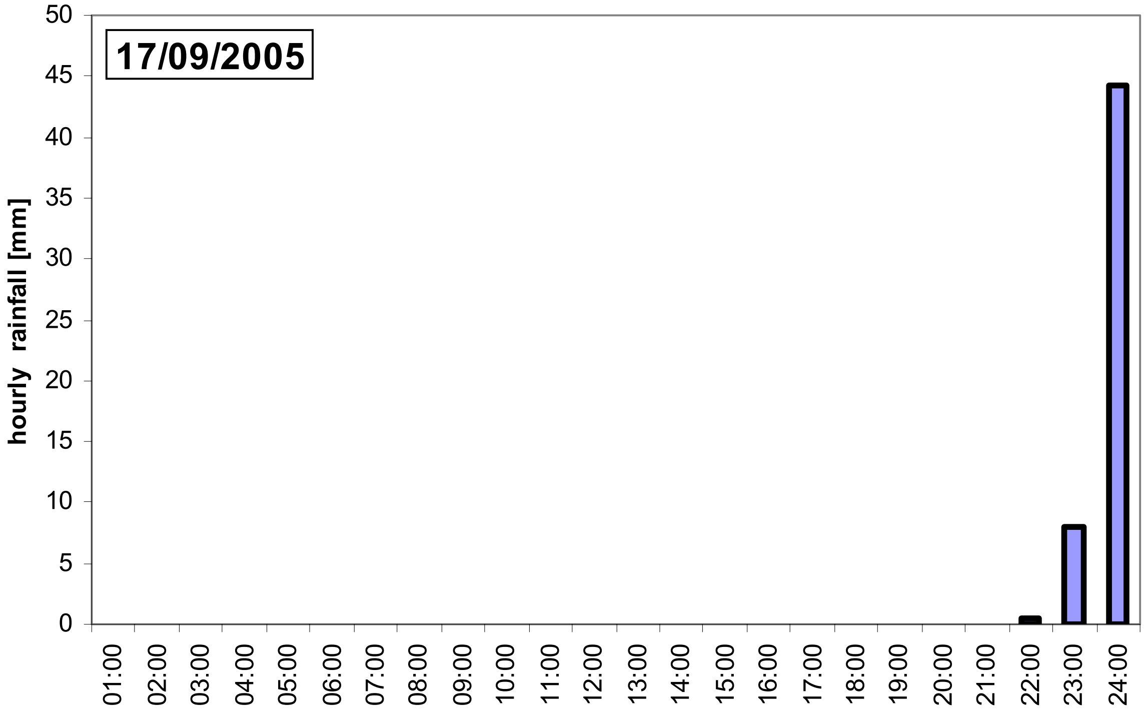

a)

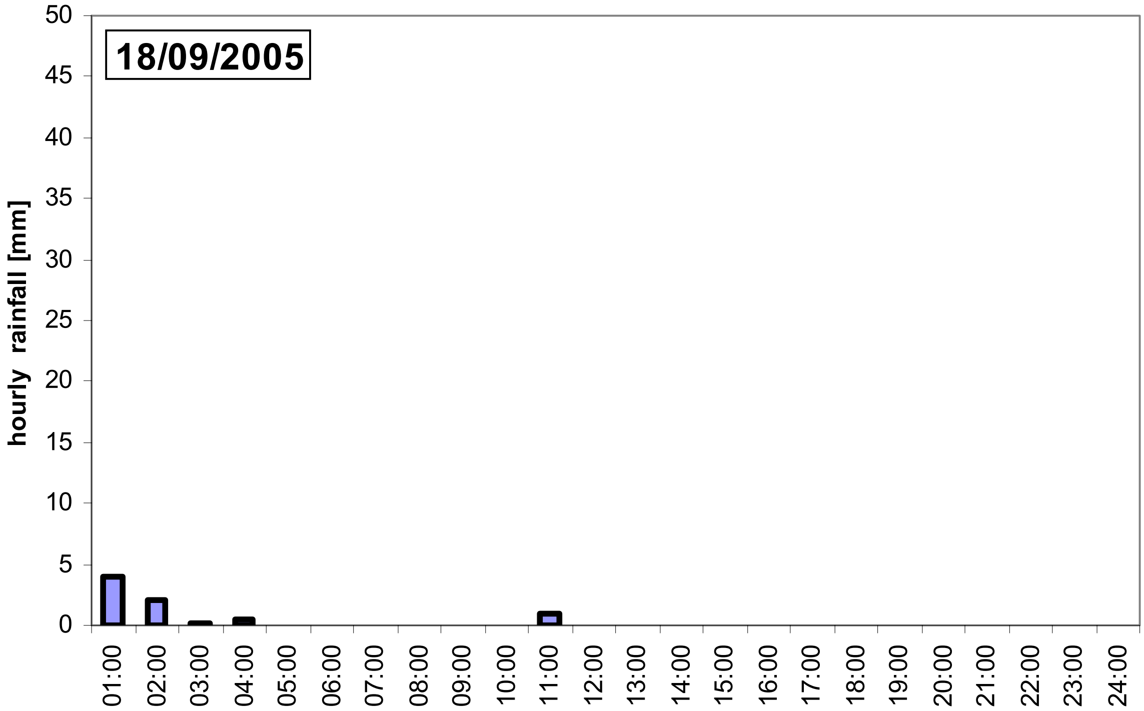

b)

Figure 2.13. Hourly rainfall measured on September 17th (a) and 18th (b), 2005

2.3 *Physical and mechanical properties of the involved soils*

The Intracaldera Phlegraean pyroclastic Deposits are the result of different hydromagmatic eruptions occurred during the past 15.000 years. They essentially consist of a sequence of fine to coarse unsaturated ashes with intercalated pumice layers. These deposits are delimited by either thin paleosols or erosional discontinuities that provide clear demarcations between the various eruptions of the recent volcanic history (< 15.000 years B.P.).
Next sections show the results of an experimental research carried out on these soils by Evangelista and Scotto di Santolo (2001). Available data regard only the finest materials (ash layers) of IPD, which represent the matrix of the coarser levels. Laboratory tests have been performed on samples, usually unsaturated, taken from boreholes drilled in different sites (Fig. 2.5), collected at depths ranging from 1.0 m to about 15.0 m. The properties can be considered representative of the shallowest deposits present at the Camaldoli hill.

2.3.1 Physical properties

Figure 2.14 shows the grain size distribution: the material ranges from fine sandy silt (indicated in figure as “A”) to well graded silty sand, and finally to sandy gravel (“D”). The clay fraction is usually less than 10% (except than for the material “A”), while the sandy fraction is usually less than 40% (except for the material “D”). This variability is related to the origin of the material, constituted by hydromagmatic eruption-style fall, flow and surge deposits. Figure 2.15 reports the physical properties as a function of the depth from the ground surface.

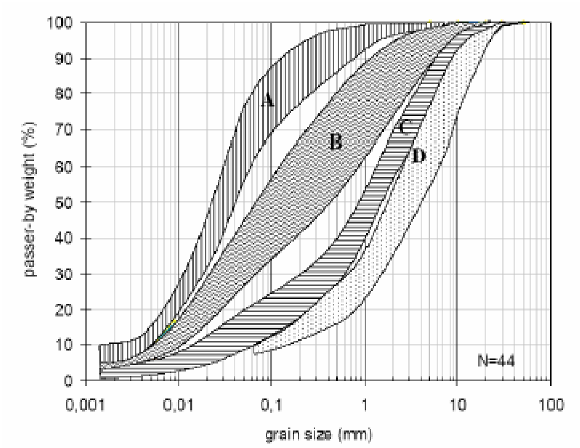

Figure 2.14. Grain size distribution curves of Intracaldera Phlegraean pyroclastic Deposits (Evangelista and Scotto di Santolo, 2001)

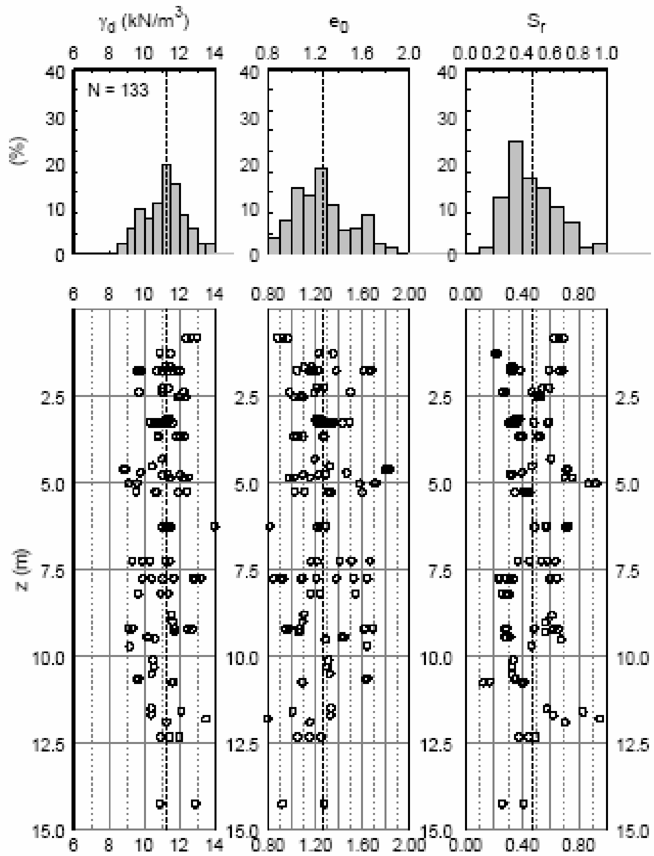

Figure 2.15. Main physical properties of Intracaldera Phlegraean pyroclastic Deposits: dry density γ_d, void ratio e_0, degree of saturation S_r (Evangelista and Scotto di Santolo, 2001)

2.3.2 Hydraulic properties

The characteristic curve of material B (Fig. 2.16) has been determined on undisturbed specimens using a Richards pressure plate and volume extractor (Scotto di Santolo, 2000). The air-entry suction $(u_a-u_w)_e$ has been assumed equal to 9.5 kPa; the highest variation has been recorded for values less than 100 kPa. The hysteresis is negligible. The experimental points have been interpolated with the correlation proposed by Brooks and Corey (1964):

$$\theta_w = \begin{cases} \theta_{ws} & \alpha \cdot (u_a - u_w) \le 1 \\ \theta_{wr} + \theta_{ws} \cdot [\alpha \cdot (u_a - u_w)]^{-\lambda} & \alpha \cdot (u_a - u_w) > 1 \end{cases} \qquad [2.1]$$

where a is the reciprocal of the air-entry suction $(u_a-u_w)_e$ and l is a dimensionless parameter representing the slope of the characteristic curve. Table 2.1 contains the parameters that have given the best fitting of experimental data.

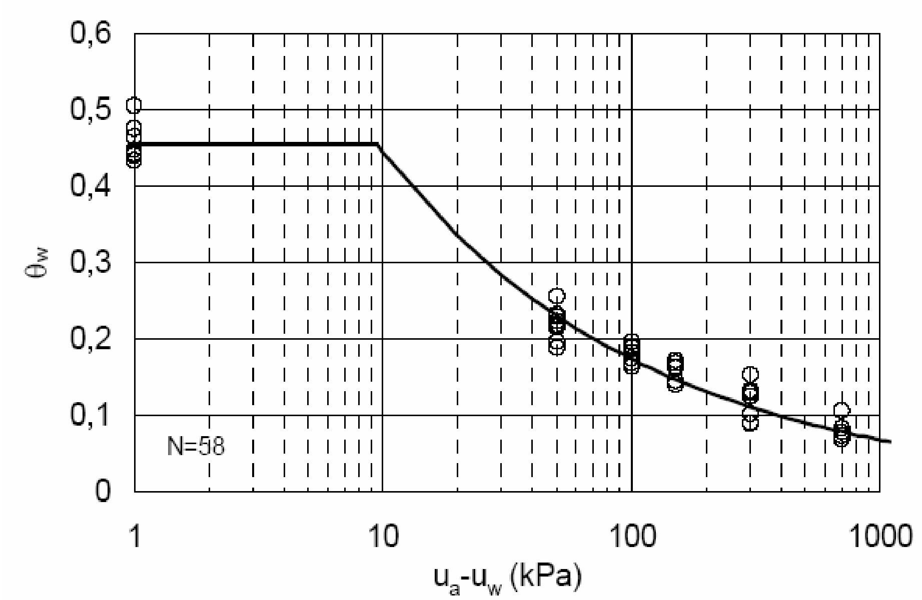

Figure 2.16. Soil retention curve of IPD – soil B (Evangelista and Scotto di Santolo, 2001)

Table 2.1. Hydraulic properties of Intracaldera Phlegraean pyroclastic Deposits

k_{ws} [m/s]	θ_{ws}	θ_{wr}	λ	α [kPa^{-1}]	**$(u_a-u_w)_e$** kPa
$5.40\cdot10^{-5}$	0.45	0.00	0.4019	0.1053	9.5

The curves fitting experimental data are also shown in Figure 2.17 in terms of relative volumetric water content Θ, defined as

$$\Theta = \frac{\theta_w - \theta_{wr}}{\theta_{ws} - \theta_{wr}},$$

where θ_w is the volumetric water content (ratio of water volume to the total soil volume), θ_{wr} is the residual volumetric water content and θ_{ws} is the saturated volumetric water content. The permeability function in terms of k_r (k_w/k_{sat}), plotted in Figure 2.17, has been obtained by the use of the indirect method proposed by Mualem (1976)

$$k_w = \begin{cases} k_{ws} & \alpha\cdot(u_a-u_w)\le 1 \\ k_{ws}\cdot[\alpha\cdot(u_a-u_w)]^{-(2+5\lambda/2)} & \alpha\cdot(u_a-u_w)>1 \end{cases} \qquad [2.2]$$

setting the saturated permeability k_{ws} equal to $5.4\cdot10^{-5}$ m/s (Table 2.1).

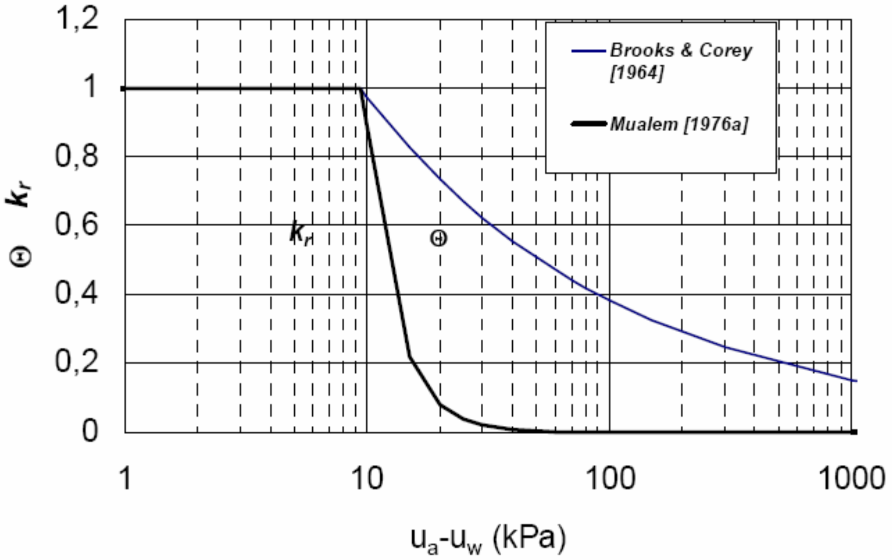

Figure 2.17. Soil retention curve and permeability function of IPD – soil B (Evangelista and Scotto di Santolo, 2001)

2.3.3 Shear strength

The shear strength has been investigated by means of drained triaxial tests (TX-CID) and direct shear tests carried out on both unsaturated and saturated specimens.
All tests performed on saturated specimens have showed the typical mechanical response of sands, i.e. brittle and dilative in case of dense specimens, and ductile and contractive in case of loose specimens. The influence of the initial degree of saturation is shown in Figure 2.18, which compares the behaviour of a saturated and of a unsaturated specimen characterized by the same dry density (γ_d = 10.76 kN/m^3), both subjected to an initial confining pressure equal to 20 kPa. The results are reported in the figure in terms of peak stress ratio η = q/p, where:

- q = s_1-s_3 is the deviatoric stress at failure;
- p = (s_1+2·s_3)/3 is the mean total confining pressure at failure;
- s_1 is the main maximum total stress at failure;
- s_3 is the confining pressure.

The figure clearly shows that a peak strength is displayed only by the unsaturated specimen. Moreover, the peak strength increases as the degree of saturation S_r decreases.
The strength envelope of unsaturated soils is strongly non linear. In fact, the mobilized friction angle φ' depends on the range of stress, rising as the confining effective stress decreases. In Figure 2.19 the peak stress ratios η=q/p and η'=q/p' (p' represents the mean effective confining pressure at failure) are plotted against the confining pressure. As it can be observed, the peak strength increases as g_d increases. The value of the critical state angle φ' is around 35°.

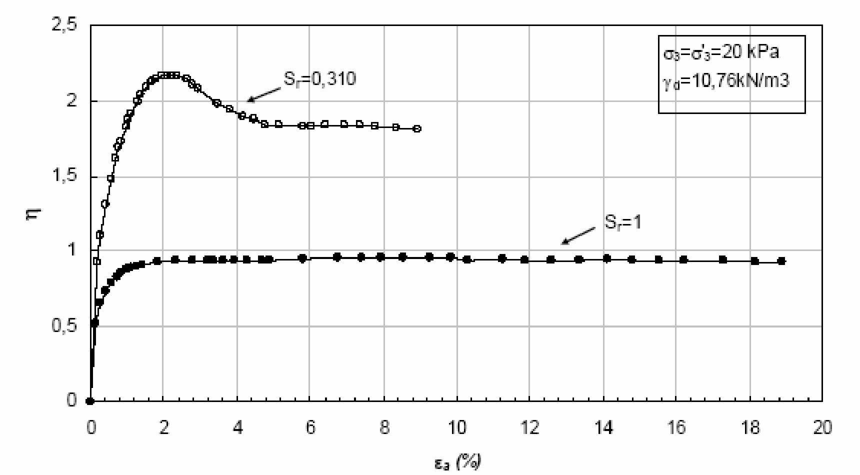

Figure 2.18. Drained triaxial tests performed on two specimens of IPD, characterized by the same dry density g_d: influence of the degree of saturation S_r on the stress-strain response (Evangelista and Scotto di Santolo, 2001)

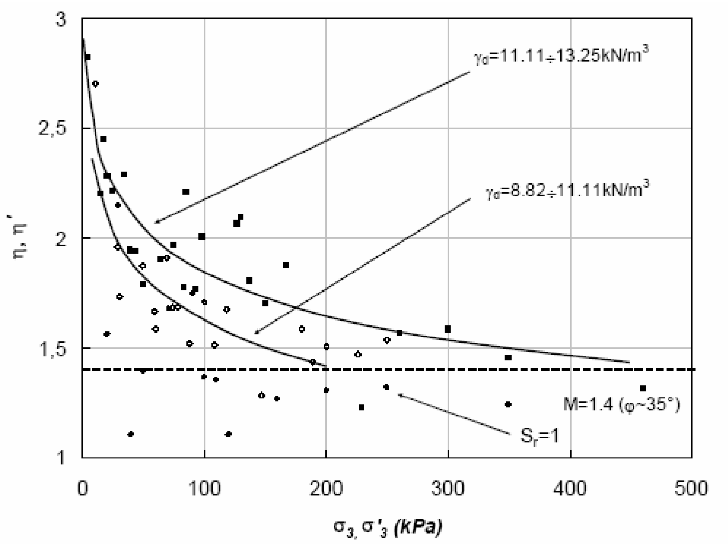

Figure 2.19. Results of drained triaxial tests performed on specimens of IPD subjected to different confining pressures (s_3, s'_3): influence of the dry density g_d and of the degree of saturation Sr on the peak stress ratio (η'=q/p'; η=q/p) (Evangelista and Scotto di Santolo, 2001)

Fredlund (1979) has furnished the following formulation for the shear strength envelope of unsaturated soils

$$\tau_{\lim} = \left[c' + (u_a - u_w) \cdot \chi \cdot tg\varphi'\right] + (\sigma - u_a) \cdot tg\varphi' \qquad [2.3]$$

where t_{lim} is the shear strength; c' and φ' are the shear strength parameters for saturated conditions; (u_a-u_w) is the matric suction, χ is a coefficient function of various factors (confining total stress, suction, degree of saturation, void ratio, etc.) and σ - u_a is the net normal stress. Plotting the equation [2.3] in the plane shear strength vs net normal stress, t_{lim} : σ - u_a, the first term of the equation [2.3]

$$c = c' + (u_a - u_w) \cdot \chi \cdot tg\varphi' \qquad [2.4]$$

represents the intercept of cohesion c (also known as *apparent cohesion*), which is a function of the matric suction. Since this latter is in turn a function of the water content, a direct relationship could be established between the water content and the shear strength. Vanapalli et al. (1996) gave to the coefficient χ the following expression:

$$\chi = \Theta^k \qquad [2.5]$$

where Θ is the relative volumetric water content and k is a fitting parameter. Substituting the previous expression [2.5], the [2.4] assumes the following aspect:

$$c = c' + (u_a - u_w) \cdot \Theta^k \cdot tg\varphi' \qquad [2.6]$$

This approach is rather attractive, because it directly associates the unsaturated shear strength with hydraulic parameters, which can be obtained by the use of standard laboratory instruments and of a pressure plate. Taking into account the critical state strength parameters c'=0, φ' = 35° and combining the soil retention curve (Θ; u_a-u_w) reported in figure 2.14, with the available results of some tests (Olivares and Picarelli, 2003) performed on the Campanian pyroclastic soils of Cervinara site (quite similar to the soils of Camaldoli site) , the best fitting can be obtained by assigning the value 2 to the exponent k (Fig. 2.17). So doing, the equation [2.6] becomes

$$c = (u_a - u_w) \cdot \Theta^2 \cdot tg\varphi' \qquad [2.7]$$

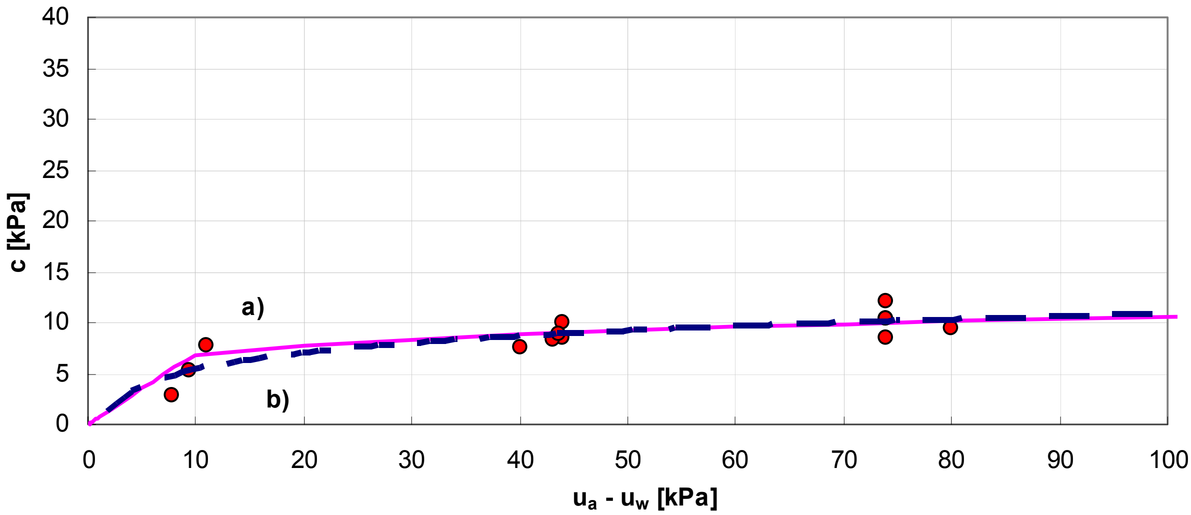

Figure 2.17. Intercept of cohesion c versus suction u_a-u_w, obtained after laboratory tests performed on the Cervinara pyroclastic soils (Olivares and Picarelli, 2003): a) fitting curve coming from equation [2.7]; b) fitting curve reported by Olivares and Picarelli (2003)

3. *The case of Nocera Inferiore*

3.1. The flowslide event of March 2005

On March 4th, 2005, at 16.00 p.m., a landslide was triggered in the northern slope of Monte Sant'Angelo di Cava mountain, located in the Nocera Inferiore town (Figure 3.1).

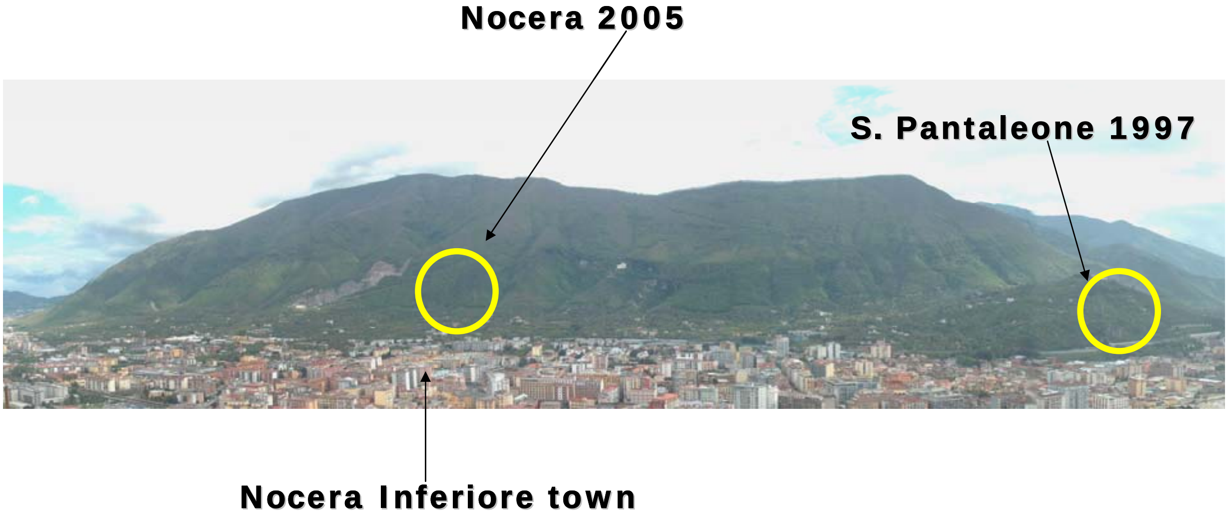

Figure 3.1. Location of the landslide occurred on March 4th, 2005

The triggering time was preceded by a cumulated height of rain over the last 24 hours of 130 mm. The event occurred on a flat slope, involving an area of 24600 m^2 and a soil mass of 33000 m^3. The landslide had a triangular shape with vertex at 390 m a.s.l and base 140 m. a.s.l.. (Figure 3.2).

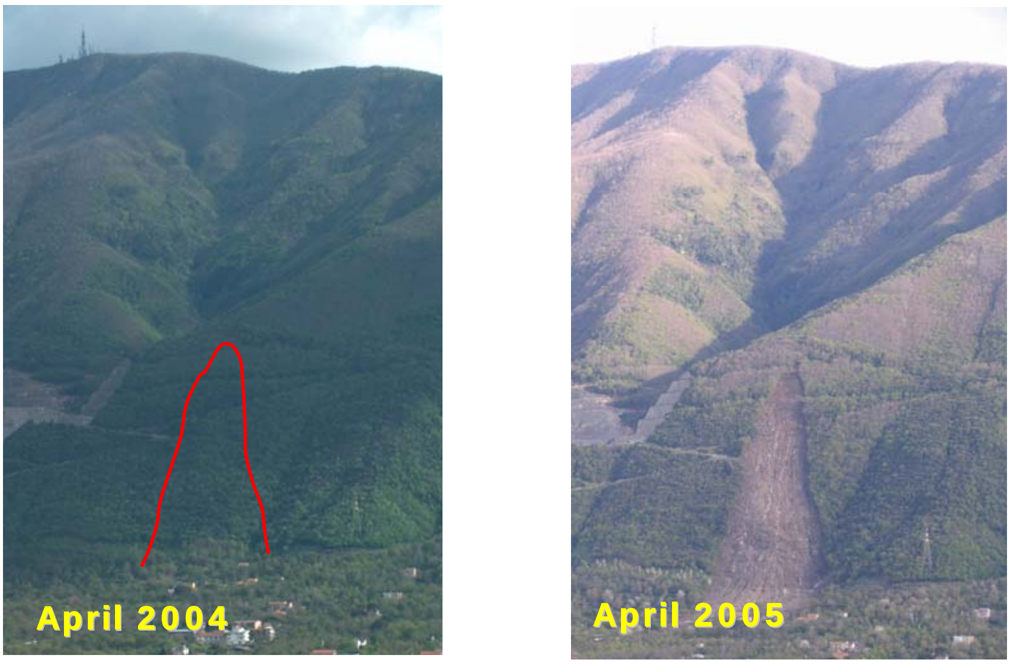

Figure 3.2. The zone of the landslide, one year before and one month after the event

The rapid post-failure movement (velocity about 12 m/s) caused the death of three people whose house was destroyed by the impact (Figure 3.3).

Figure 3.3. Damages caused by the Nocera 2005 flowslide

At the toe of the slope the soil mass spread on a wide area (20000 m^2) at elevation ranging between 140 m.a.s.l. and 100 m a.s.l..
The average inclination of the slope is of 36°. At the slope top the angle is higher (40°) and two roads, functional to a cave located in a nearby site, go through the slope.
The slide involved pyroclastic soils mixed with carbonatic fragments. The carbonatic bedrock is located at depths ranging between 1 and 3 meters and is significantly fractured. Layers of pumices are often included within the covers. Some significant morphological jumps feature the bedrock, making the pyroclastic layer discontinuous and characterized by steps. The landslide is likely to have triggered in the upper zone and propagated downward.
The Nocera 2005 flowslide is the last and more significant event among a large number of events occurred around the Nocera Inferiore town in the last decades. Table 3.1 outlines the main flowslides occurred in this area, with their fall height, projection distance, reach angle and the landslide volume.

The most significant and documented flowslide preceding that of Nocera 2005 occurred in the nearby hill of S. Pantaleone hill in 1997 (see Figure 3.1).
It is worth noting that in the same day of the Nocera 2005 landslide, many others minor slope failures occurred in the same zone. In particular, a small flowslide was triggered in the S. Pantaleone hill.

Table 3.1. Most significant flowslides triggered in the Lattari mountains during the last decades (de Riso et al., 2005)

N.	Flowslide	Date	Fall height (m)	Projection distance (m)	Volume (m^3)	Angle of reach (°)
1	Scrajo	23/11/66	220	300	10.000	36
2	M. Pendolo	02/01/71	205	375	7.500	28
3	S. Pantaleone	06/03/72	90	180	5.000	26
4	Mitigliano	16/02/73	200	272	9.000	36
5	Palma C.	22/02/86	185	400	8.000	25
6	S. Pantaleone	10/01/97	135	240	4.500	29
7	M. Pendolo	10/01/97	125	210	4.500	31
8	Rimonte	10/01/97	130	135	750	43
9	S. Egidio	10/01/97	215	500	10.000	23
10	Bracigliano	12/04	220	468	-	25
11	Nocera	04/03/05	295	530	33.000	29
12	M. Faliesi	04/03/05	200	400	15.000	27

3.2. *Geological and geomorphological setting*

Detailed geological studies have been conducted in the Nocera landslide area through field investigations integrated by stereoscopic analysis of air photo taken before the event and by geophysical tests.
Particular attention has been paid to the determination of the thickness of pyroclastic covers. Near the landslide area, covers are in between 2 and 4 meters. In the triggered zone the slide plane is located within one of the pumices layers contained in the pyroclastic sequences.
The pumice layer found in the upper zone disappear completely in the medium and lower parts of the slope. The lower part of the slope is shaped by man made steps. Figure 3.4 plots a stratigraphic section of the upper part of the slope.
The geolitological map of the slope, i.e the geological map without considering the covers, is reported in Figure 3.5. It provides information about the boundary condition at the bottom of the pyroclastic layer. Due to the carsified and fractured state of dolomitic rocks, it is possible to assume a free draining condition.
Figure 3.6 is a map of the cover thickness.
The geomorphological map (Figure 3.7) provides information about the landslide types. In this area has been recognized the importance of the so called ZOBs (the Zero Order Basins) where pyroclastic covers are gentler and often present a very high porosity. The smaller slope angle facilitates the collection of a high amount of water during rainfall events. ZOBs are connected with channels. These can originate channelled landslides, whose travel distance can be even of some kilometres. Figure 3.7 shows that the 2005 flowslide was triggered on open a flat slope bounded laterally by two channels.
The map of slope angles (Figure 3.8) is important because these are related to the probability of landslide occurrence. Based on geological and geotechnical studies

(Picarelli et al., 2008) the highest probability is for slope angles between 32° and 37°. Figure 3.8 shows that most inclination values are included in the range of high probability of flowslide occurrence.

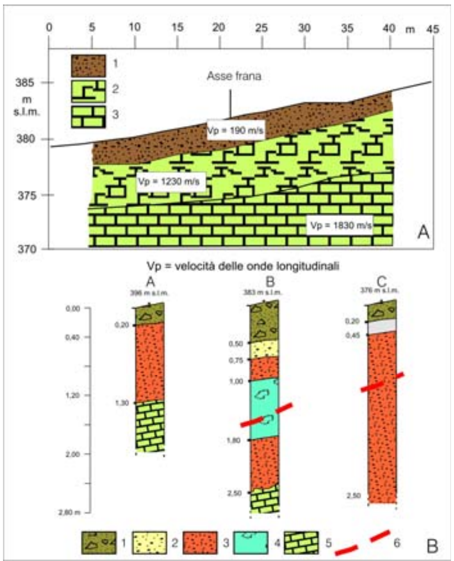

Figure 3.4. Stratigraphic section at the top of Nocera 2005 slope

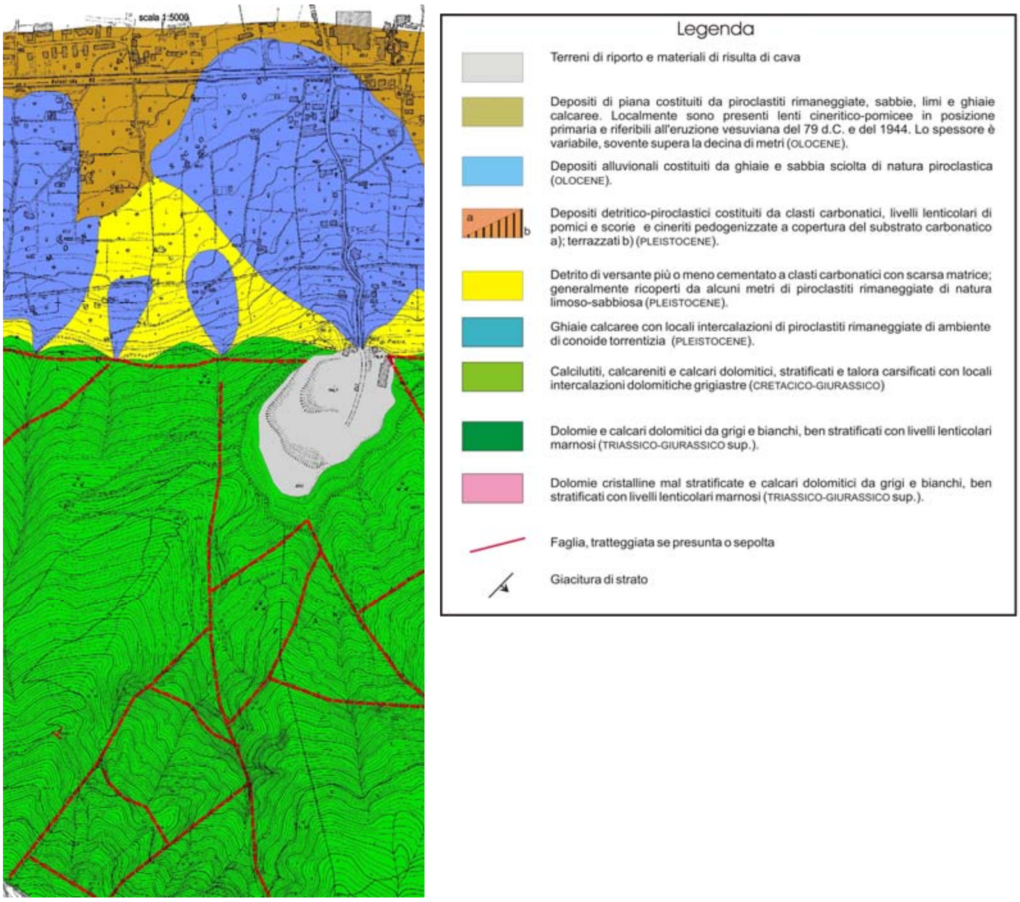

Figure 3.5. Geolithological map of the Nocera 2005 flowslide area

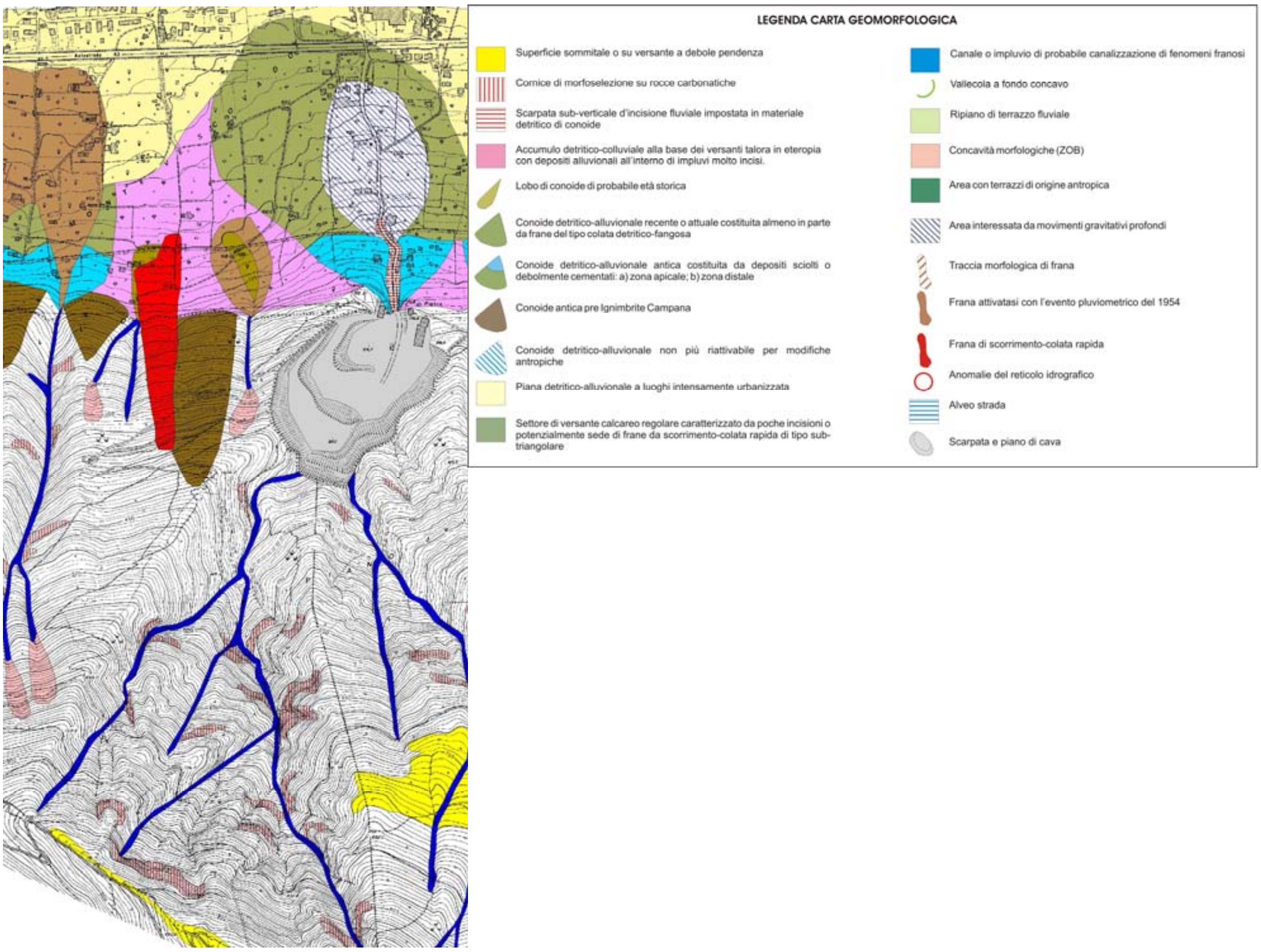

Figure 3.6. Geomorphological map of the Nocera 2005 flowslide area

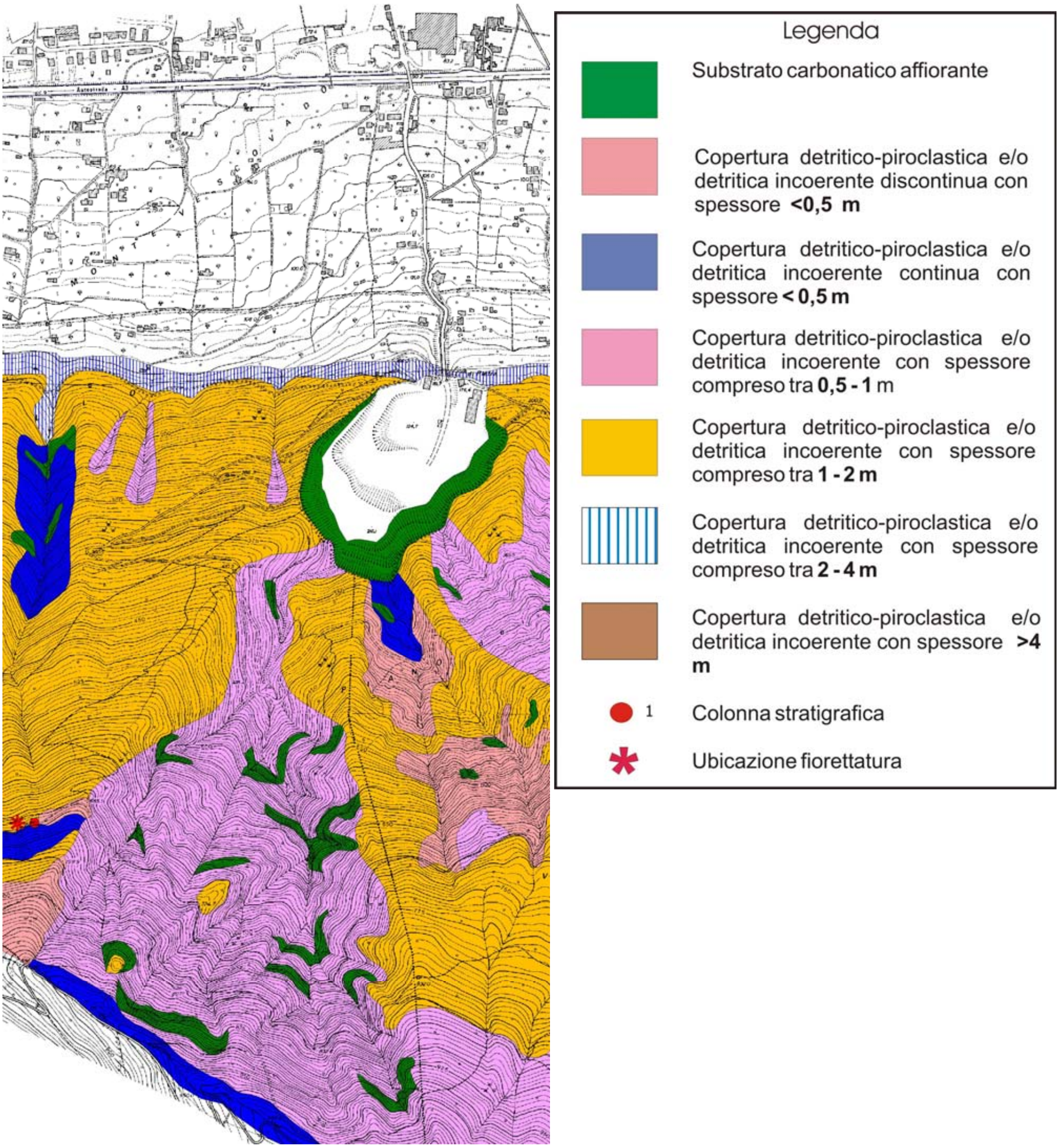

Figure 3.7. Map of thickness of pyroclastic layers in the Nocera 2005 flowslide area

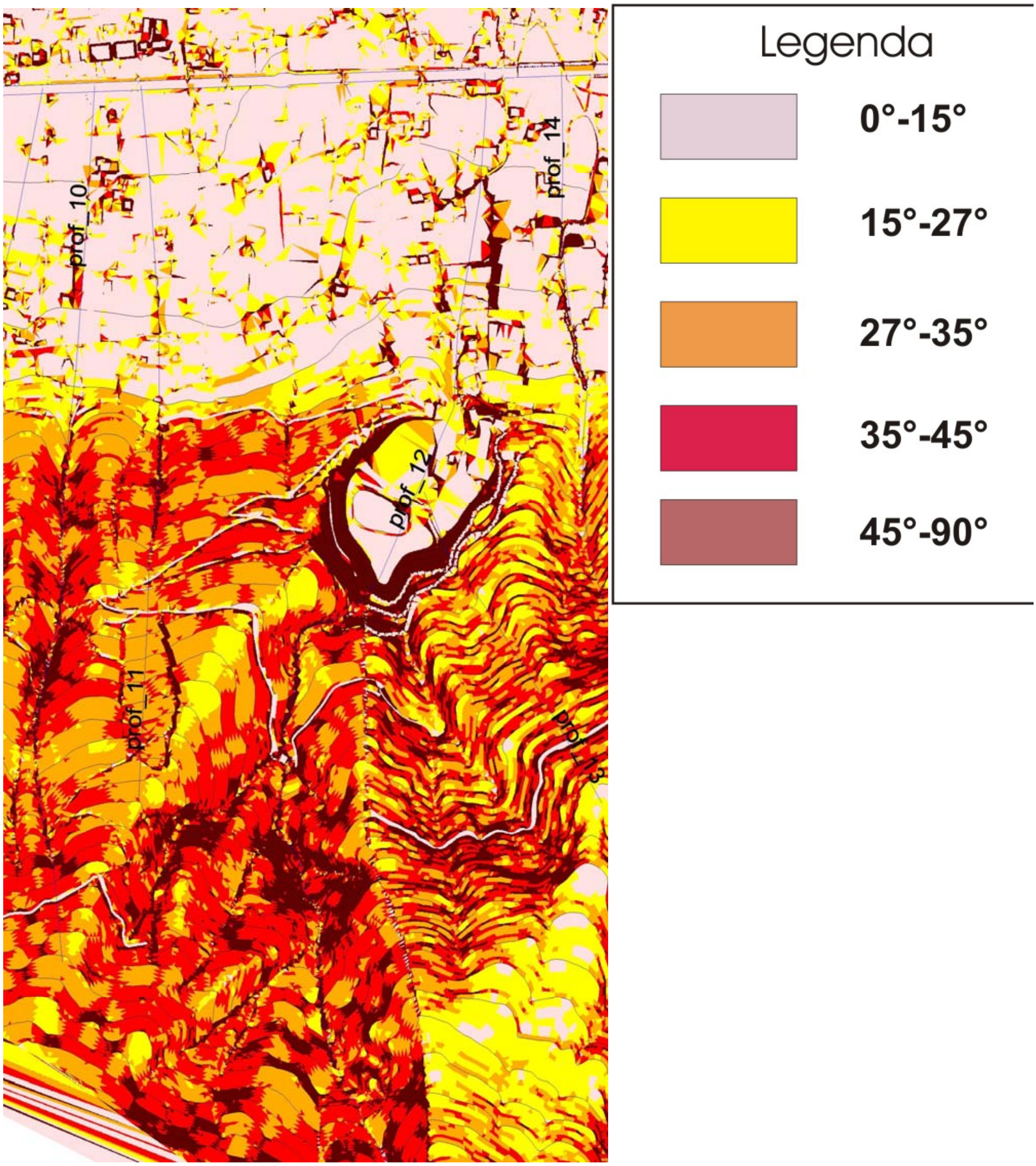

Figure 3.8. Map of slope inclinations in the Nocera 2005 flowslide area

3.3 Physical and mechanical properties of the involved soils

The pyroclastic sand from Nocera

An experimental program was carried out to determine the hydro-mechanical behaviour of pyroclastic soils involved in flowslide events. The material used in this experimentation was taken from a site which lies close to the foot of the Nocera hill, where the flowslide took place. Here is located the deposition zone of previous slides.
As reported in Fig. 3.9, from the bottom to the top, the following layers have been singled out:

- fractured calcareous rocks;
- volcanic ashes (A), homogeneous, colour from light brown to yellow;
- pumices (B);
- pozzolana (C) colour light brown, containing some roots;
- pyroclastic layer (D), containing a thick roots network, deriving from shrubs growth.

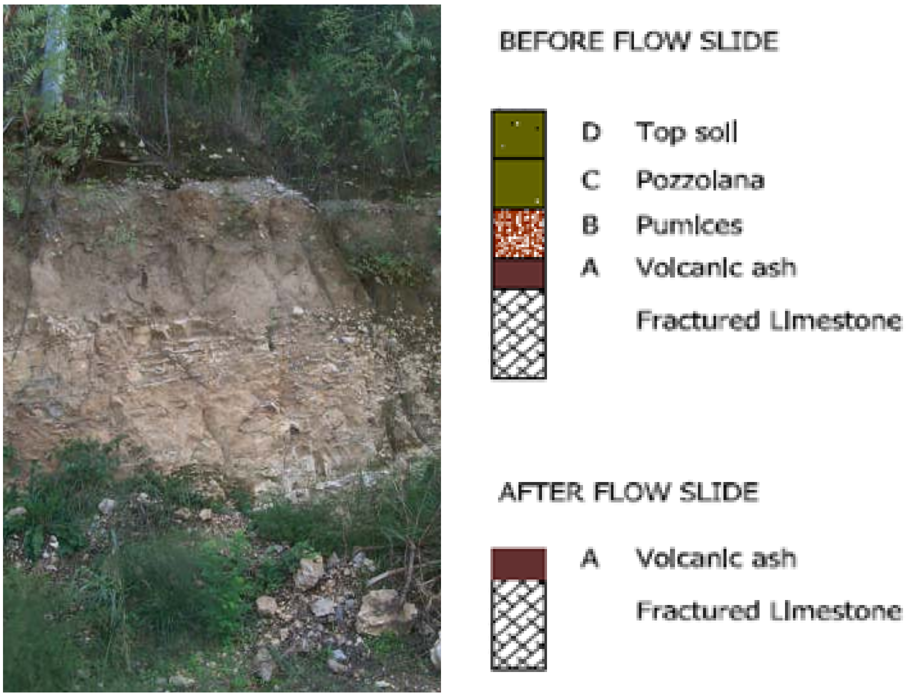

Figure 3.9. Typical soil stratigraphy of the slope involved in the flow slide before and after failure

The ash layer, thanks to its grading curve in which the fine content prevails, is capable to preserve its water content almost unchanged also on summer. The pumices layer, is not present everywhere along the slope: not in the steepest zones, were the flowslide was triggered.
The grain size curves are shown in Figure 3.10. The fine content of specimens taken from the upper side of the hill (curve plotted with continuum line) is very different from the one of samples taken from the lower side of the hill (dashed curves). In fact, in the first case the sand matrix prevails over the clayey matrix, while in the second case the silty content is prevalent. This distribution is consistent with the material exchange

mechanism that take place during the soil movement, between the soil mass and the sliding layer. In fact, during the slide, the soil flow is not strong enough to carry downs the bigger particles, that set down along the way. Instead, the finest particles stay suspended in the soil mass, and set down only at the tip of the slump.

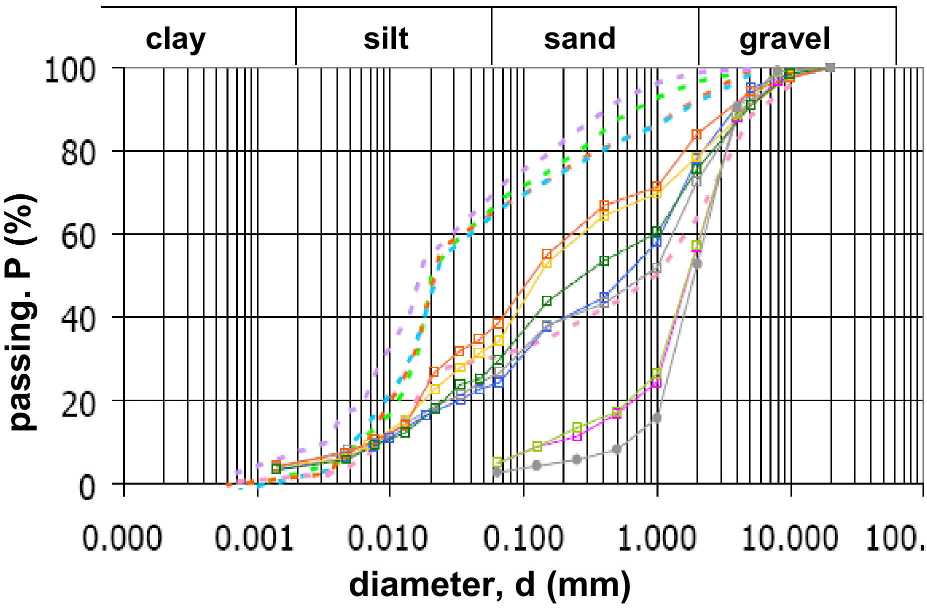

Figure 3.10. Soil grading curves

The soil particle specific weight is equal to 2.68 g/cm^3 .
The soil plasticity of the soil is barely zero, except for the specimen taken from the downslope zone, in which the higher fine content manifests itself in a Ip=10.9%, w_L = 45.11% and plasticity limit w_P = 34.20%. An organic fraction of 5% was found.
The material utilized in the laboratory investigation can be classified as a silty sand and/or as a gravelly sand (ASTM D2487-00).

Stress state and hysteresis influence upon the SWRC of a silty sand using the modified oedometer apparatus

In engineering applications soil can be subjected to stress levels and bulk density conditions that may result in a family of soil-water retention curves (SWRC) instead of a single characteristic one. Furthermore, climate changes typically generate alternate drying and wetting of the near-surface soil, reflected as hysteresis of their water retention properties. All the above must be carefully considered when using SWRC in the determination of flow models parameters for environmental geotechnical applications.
A modified oedometer has been recently developed at the Dipartimento di Ingegneria Geotecnica of the Università degli Studi di Napoli Federico II to obtain experimental data which may allow to investigate the influence of the above mentioned variables upon SWRCs of the mentioned above pyroclastic soils (silty sand).
Opposite to what was believed in the past, apart from the method adopted to represent the water retention capacity of a soil [i.e. matric suction (u_a - u_w) against gravimetric

water content (w) or the volumetric water content (θ) or the degree of saturation (S)], a unique SWRC does not exist. As a matter of fact, the variables controlling the water retention capacity of the soils generate a family of curves instead of a single characteristic one, depending on the previous suction history, the volumetric state or stress level and history.
The water content at a given suction for a wetting path is less than that for a drying path (i.e. SWRC hysteresis). Alternate stages of drying and wetting form an infinite number of scanning curves inside a main hysteresis loop. The name of the various branches of the SWRCs are well known and are indicated in Figure 3.11. The air-entry value[1] (AEV), and the residual moisture content[2] (θ_r) are parameters characterising the SWCR. The AEV varies for every SWRC, while the θ_r seems to be not influenced by the hydraulic hysteresis (Fig. 3.11).

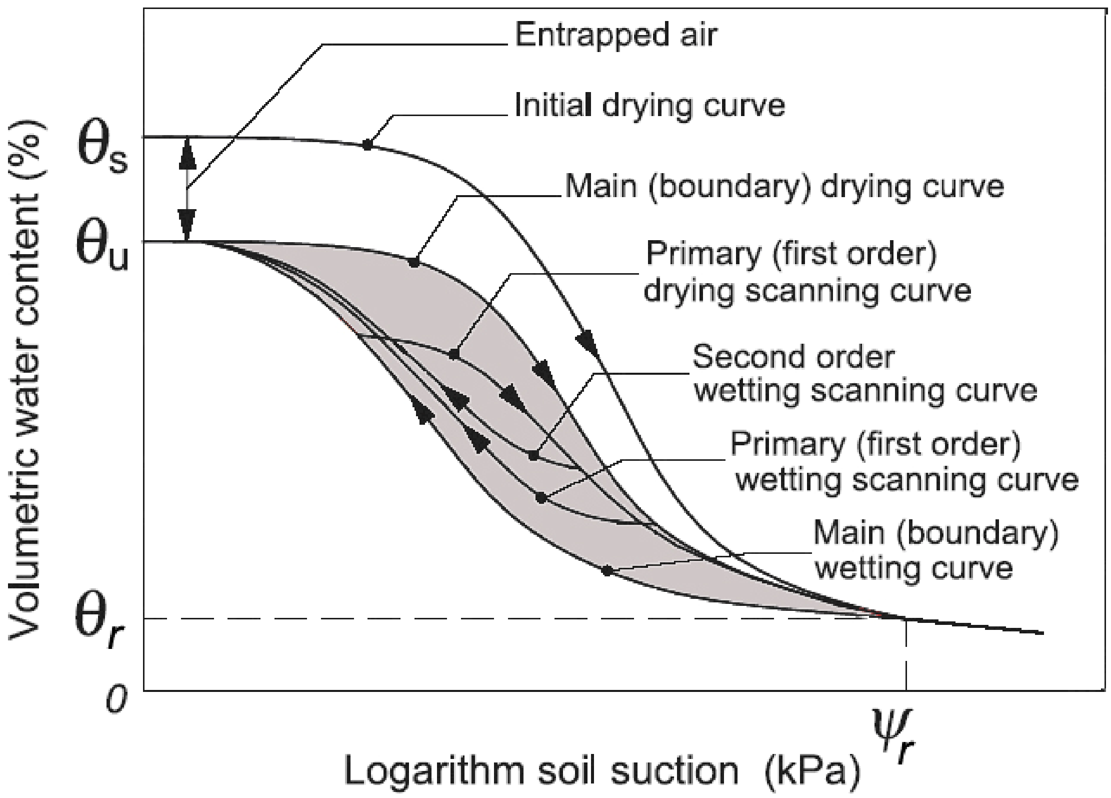

Figure. 3.11. Commonly used definitions for hysteretic SWRCs (after Vereecken et al., 1995)

Furthermore, the SWRC is often defined considering only suction as stress state variable and neglecting the effects of volume changes on wetting and drying cycles. Experimental studies, however, have demonstrated that the soil state is also important and needs to be considered in defining its water retention capacity (Ho et al., 2006). Other data (Vanapalli et al., 1999; Romero and Vaunat, 2000) also demonstrate that given a single soil type, compaction method may influence its fabric and void ratio,

[1] The air-entry value of the soil is the matric suction where air starts to enter the largest pores in the soil.
[2] The residual water content is the water content where a large suction change is required to remove additional water from the soil.

causing significant changes in its water retention properties. In numerical simulations, however, net stress and hysteresis effects on water retention properties of soils can lead to significant discrepancies between prediction and in situ observational (Vereecken et al., 1995, Mitchell and Mayer, 1998).
Recently devices able to face all the mentioned aspects of soil behaviour have been developed, capable of applying prescribed values of stress, flushing diffused air and measuring volume and water content changes with reasonably precision (Ng and Pang, 2000; Leong et al., 2004; Wang and Benson, 2004; Padilla et al., 2005).

In this section, the influence of stress state and hysteresis upon the SWRC of a pyroclastic silty sand is discussed. The experimental measurements have been obtained at the Dipartimento di Ingegneria Geotecnica of the Università degli Studi di Napoli Federico II using a modified oedometer: the main features of the device, including pressure/volume controllers and flushing method, are also described in this report. In addition, filter paper test was used to perform some complementary matric suction measurements, the obtained data are also presented.

Experimental procedure and results

The testing program to determine the SWRC was carried out using is a Wissa oedometer (Wissa and Heiberg 1969) modified to control matric suction (Rampino et al., 1999), to measure water content changes (Rojas et al., 2006) and to control all the stress-strain variables relevant to unsaturated soil mechanics. The matric suction, controlled with axis-translation technique[3] (Hilf, 1956), is applied in finite increments in order to measure SWRCs and maintained constant until the soil specimen reaches an equilibrium state.
The apparatus is capable to hold samples of 79,5 mm in diameter, and 25,0 mm in height. Its capacity to measure matric suction is restricted by the use of a 500 kPa high air entry value disk (A in Figure 3.12). The pore air pressure, u_a, is applied at the top of the specimen and pore water pressure, u_w, at the specimen base. Both are driven by Firechild regulators (B and C in Figure 3.12, respectively) and measured by pressure transducers (D and E). The pore water pressure is generated by applying air pressure on the air-water interface inside the twin burettes (F) of Figure 3.12. A load piston (G) connected to the top cap imposes vertical loads. The applied stress is registered by a load cell. The axial strains are measured by a linear variable displacement transducer, LVDT (I).
The pore water volume variation is measured by a system constituted by two double walled burettes connected to a Differential Pressure Transducer (DPT) (J in Figure 3.12). One burette is connected to the drainage line and the another one acts as a reference for the pressure measurements from the DPT. The water level variations due to evaporation at the water-air interface in the burettes is balanced by the system symmetry.

[3] The axis translation technique consists in applying positive values of pore-air and pore-water pressures allowing to drive them in the positive range and to measure them with standard transducers. In nature unsaturated soils are generally subjected to atmospheric pore-air pressure and negative pore-water pressures.

The saturation of the water drainage pipelines is ensured placing the high air-entry value ceramic disk at the base of the sample and flushing periodically the drainage cicuit. Flushing is obtained by a peristaltic pump (K) acting on the drainage line: the pump flushes water through a spiral circuit caved inside the base pedestal, drive air bubbles into the measurement burette and expel them through the free water-air interface. The arrows on Figure 3.12 shows the path of flushing.

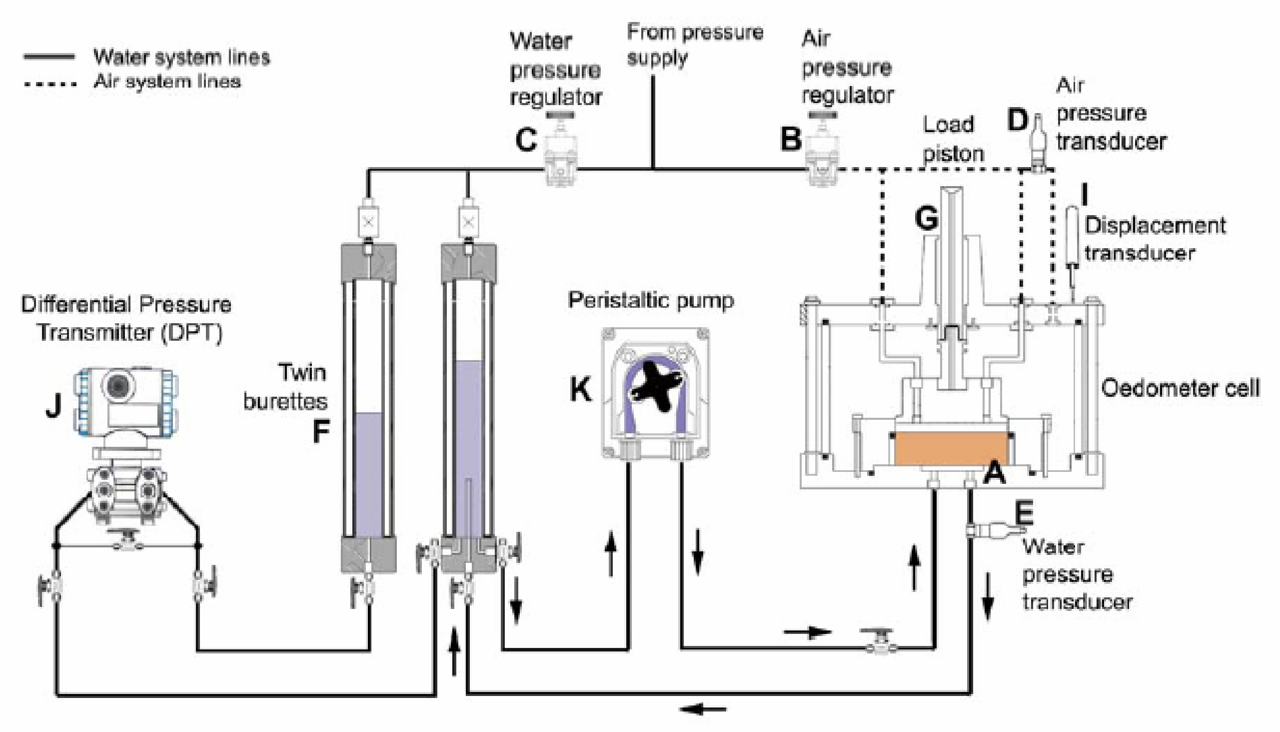

Figure. 3.12. Modified Wisa oedometer for unsaturated soils.

Prior to any SWRC determination, the specimens are loaded up to a prescribed net axial stress (σ_v - u_a) equal to 50 or 100 kPa; the purpose of this preliminary loading is to compensate the effects of volume changes during the subsequent stages of the test. As a matter of fact, two experiment procedure can be used. The first one consists in SWRC determined at constant (σ_v - u_a). The second one, consists in constant void ratio (e) SWRC determination; in the latter case reduction in e that may result from suction changes are generally compensated by swelling produced through (σ_v - u_a) decreases.

A personal computer connected to the load cell and to a digital ram regulates the stress level using a feed-back procedure.

The test program consisted of monotonic drying and wetting tests and cyclic tests performed to obtain families of SWRCs. Table 1 summarizes testing condition and sample properties. To generate monotonic drying and wetting cycles, air gauge pressures u_a of 10, 20, 50, 100, 200, 300 and 400 kPa have been imposed in steps under a constant value of water gauge pressure u_w of 50 kPa. Secondary cycles performed in order to evaluate the hysteresis were generate changing the u_a in a range of 2 to 463 kPa.

Table 1. Experimental program and main sample characteristics

Test	Method	Net axial stress (σ_v - u_a) [kPa]	Measurement path	Initial sample characteristics‡ Porosity n	Dry unitary weight γ_d [kN/m^3]	Water content w [%]
CNAS50m	Axis translation	50	monotonic	0.57	11.5	51.2
CNAS100m	Axis translation	100	monotonic	0.55	11.9	44.9
CNAS50h	Axis translation	50	hysteretic	0.56	11.8	42.1
CNAS50h	Filter paper	0	drying points	--	--	--

‡ values after pre-loading process.

The filter paper test were also performed to measure matric suction higher than 500 kPa (i.e. higher than the actual maximum capacity of the oedometer). In particular, at the end of test CNAS50h the soil sample was removed from the oedometer and used to perform suction measurements with filter paper method.

Figure 3.13 shows experimental data and fitting curves for monotonic water-retention tests at different stress level; tests CNAS50m and CNAS100m refer to a net axial stress of 50 kPa and 100 kPa, respectively. The data have been fitted using van Genuchten (1980) model.

According to previous studies on the effects of net axial stress on SWRCs (Ho et al., 2006), the CNAS100m cycle presents a lower desorption rate, a higher absorption rate, an AEV slightly higher, and a smaller hysteresis loop compared with CNAS50m cycle.

As illustrated in Table 1 the initial porosity and water content of CNAS50m sample are higher than the corresponding values of CNAS100m sample. As expected, SWRCs obtained from the tests indicate that as the sample porosity decreases, the absorption rate increases and the desorption rate decreases (Ho et al., 2006; Anderson and Stormont, 2006). Thus, referring to curves reported on Figure 3.12, an increment on axial stress effect due to a superposition with porosity effect should be considered.

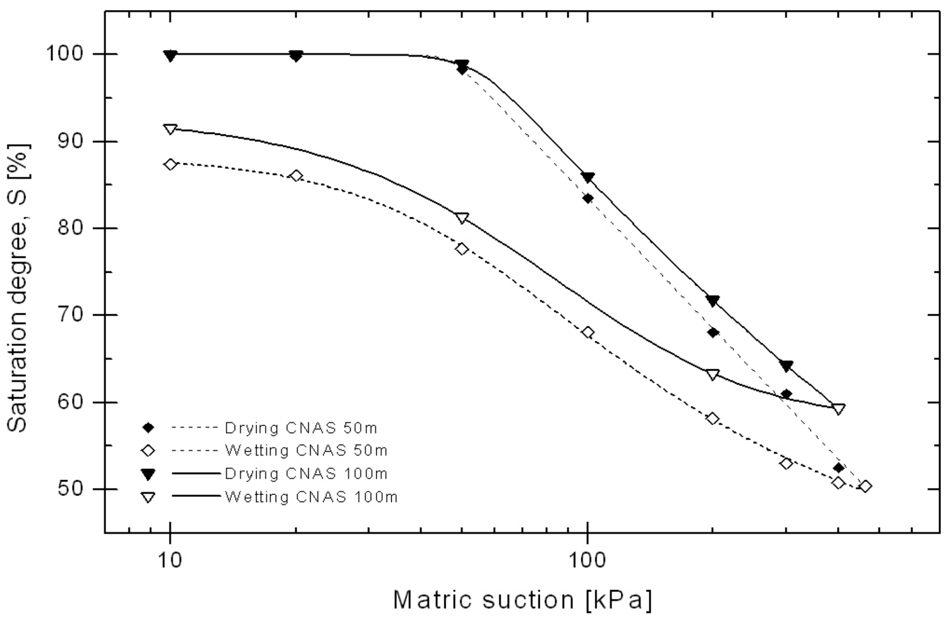

Figure. 3.13. Comparison of SWRCs between specimens under different net axial stresses

During CNAS50h test, the influence of drying and wetting cycles history on "main" SWRC was evaluated. The soil sample was subjected to 4 drying and 3 wetting cycles between 2 kPa to 463 kPa of suction (Fig. 3.14). According to Ng and Pang (2000), the size of the hysteresis loop is larger in correspondence of the first cycle and tends to become independent of the drying and wetting history after the first suction cycle. In other words, as the number of drying and wetting cycles increases, the volumetric water content at low suction values decreases, but the rate of reduction is drastically diminished. The trapped air in the pore space after the first wetting cycle may cause the observed effect (Haines, 1930). The two last cycles (i.e. 3rd wetting and 4th drying) were performed to obtain scanning curves. As expected, the scanning loop ends in the same point where started (i.e. matric suction = 200 kPa and volumetric water content = 30.9 %). Thus, a cycle that generates a scanning loop does not produce irreversible water content or porosity changes.

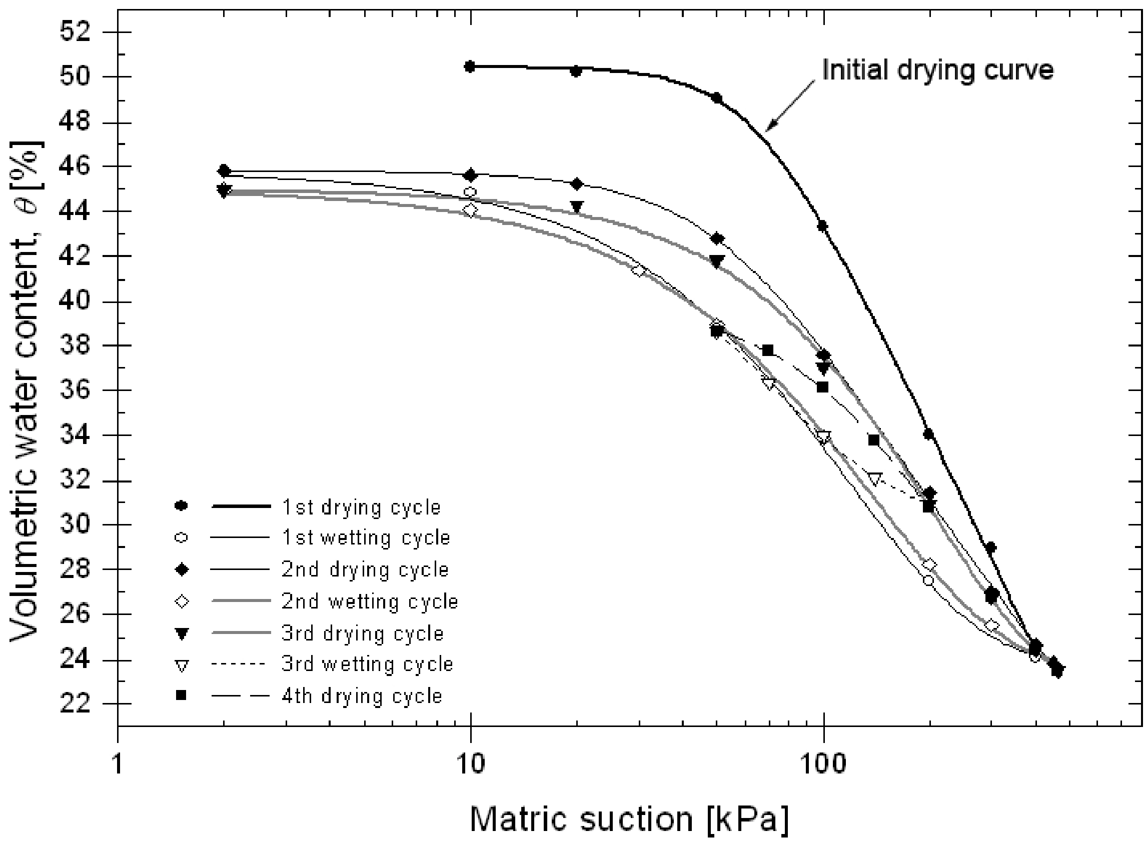

Figure 3.14. Family of SWRCs corresponding to CNAS50h test

The 1st drying cycle is defined as initial drying curve, representing a desorption process when it starts from a fully-saturated condition. Due to sample structure and the maximum matric suction that the equipment can apply (i.e. 500 kPa), the residual condition was not reached. So, θ_r (which is input data in all hysteretic models) is

missing, wetting cycles do not represent the main wetting curve, and that drying cycles do not represent the main drying curve.
The suction measurements using filter paper method have been used to attempt a solution of the mentioned problems. Data collected are shown on Figure 3.15. Just three measures were performed due to the long time (15 days) required to equilibrate the matric suction for every filter paper measurement. During the test, the net axial stress was not controlled, however, a good agreement exists between the modified oedometer and the filter paper data.
Based on filter paper data, approximate indications on the main loop corresponding to CNAS50h sample can be obtained as shown in Figure 3.15: experimental data seem to demonstrate that loop previously discussed (i.e. 3rd and 4th drying cycle and 2nd wetting cycle) can be classified as an external loop. In other words if θ_r would have reached and wetting would be performed, the curve A of the Figure 3.15 would be obtained as main wetting and the curve B as main drying. However, it's expected that in many engineering applications the soil will never experience suction value greater than achieved in the loops detected with the modified oedometer. In this case (i.e. maximum suction experienced in situ = 463 kPa), the main loop does not reflect the field moisture-suction variations.

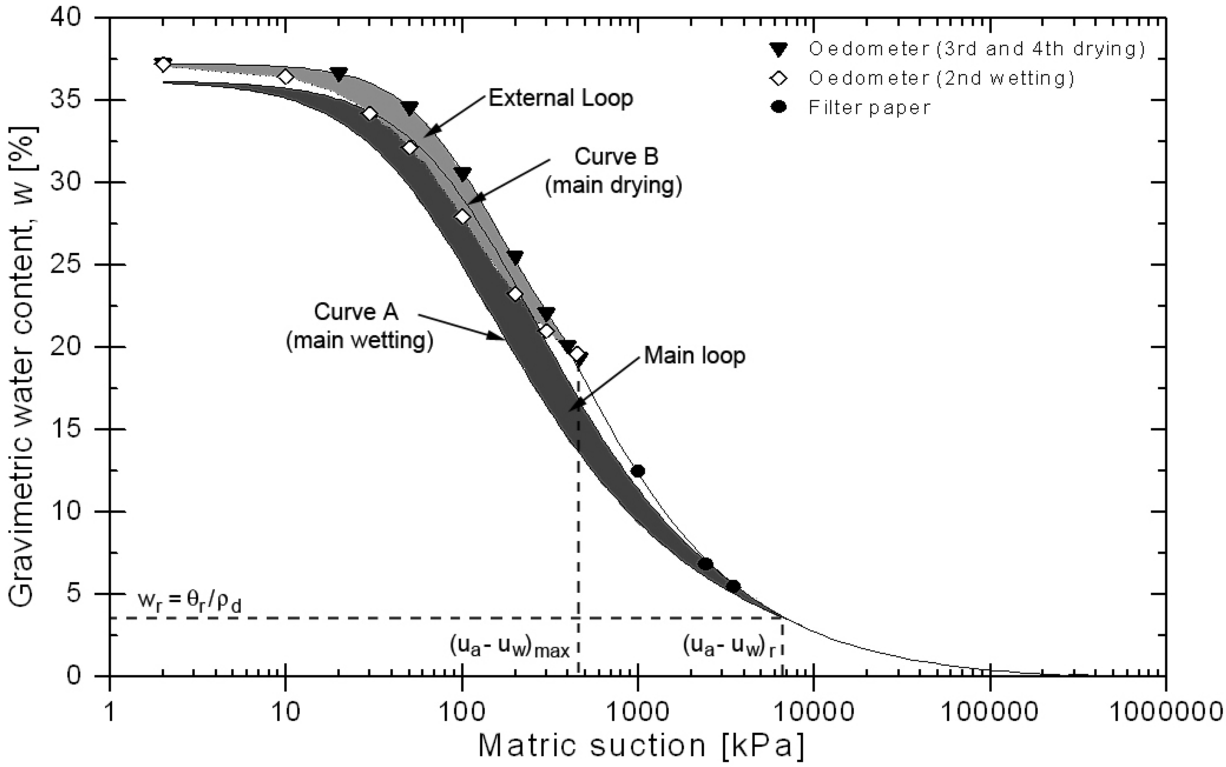

Figure 3.15. External loop and theoretical main loop

Conclusive observations
Monotonic and hysteretic SWRCs of consolidated specimens were tested under different applied stress levels using of a modified oedometer, which allows the application of controlled levels of vertical net stress and volume change

measurements. For the particular soil tested and testing conditions the observations and conclusions resulting from the collected data can be summarized as follows.

As vertical net stress increases, SWRC presents a lower desorption rate, a higher absorption rate, and a smaller hysteresis loop.

Vertical net stress seems to not significantly affect the AEV.

The size of the hysteresis loop is quite larger in the first cycle, and seems to become independent of the drying and wetting history after the first cycle.

For soils that never experienced the residual water content, θ_r, the zone inside the main loop does not reflect the zone where moisture-suction varies in field. Then, for some practical applications the understanding of θ_r is not mandatory. In some cases, the models that require θ_r as a fundamental piece of information for hysteresis analysis, maybe are not useful for real applications.

The SWRC is quite highly dependent of stress-strain level and previous suction history, limiting the role of predictive models for SWRC estimation to a preliminary guide for testing program.

3.4. Monitoring data

For the Nocera Inferiore site, daily rainfall data are available from January 1951 up to the end of 1999, thanks to the hydrological annuals of “Servizio Idrografico e Mareografico”. Hourly data are available from January 2000 up to March 2005 from rain gauges installed by Società Autostrade Meridionali. Data from 1999 are plotted in Figure 3.16 for different cumulated time periods. In each plot, a triggering threshold is also indicated. The threshold represents the minimum value associated with a flowslide triggering during the period from 1950 to 1999, among the flowslides occurred in the Nocera Inferiore site, on December 8th, 1960, March 6th, 1972 and January 10th,1997. It’s worth noting that those landslides didn’t occur during the beginning of the fall, which is typically characterized by the highest values of the rain intensity, but were triggered later because of the rain cumulated during the successive several weeks. This suggests that the hydraulic properties of pyroclastic soils are such to make the soil water content sensitive to the rains of the last few months. This feature is also supported by the difference between threshold and cumulated rains associated with the Nocera 2005 flowslide, which is very high in correspondence of rains cumulated over few days (Figure 3.16), while it is minimum for rains cumulated over two months (Figure 3.20).

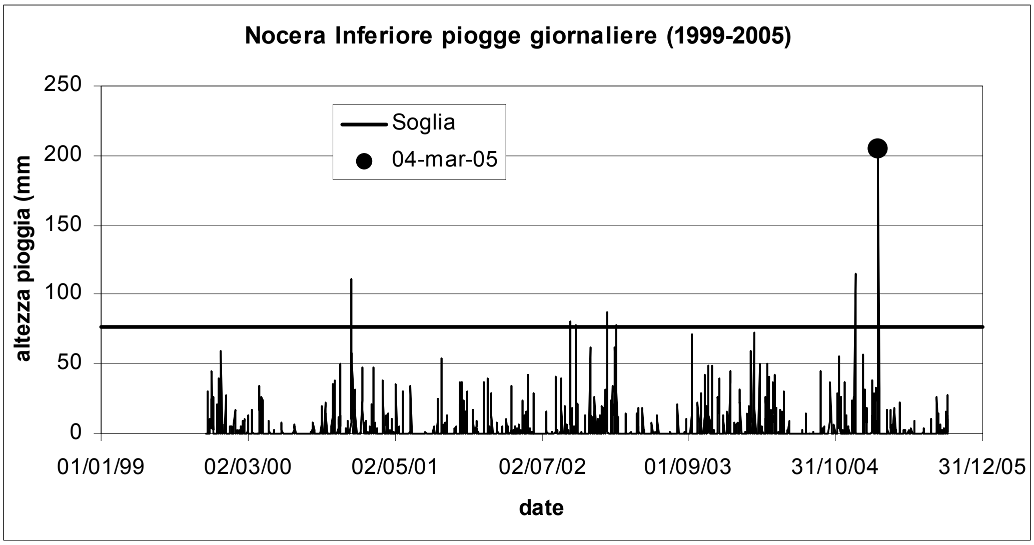

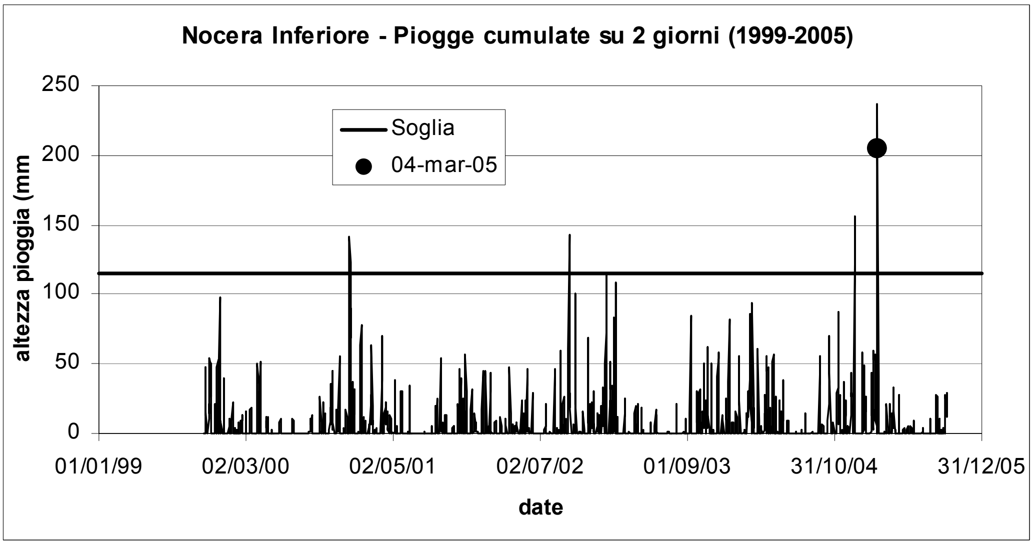

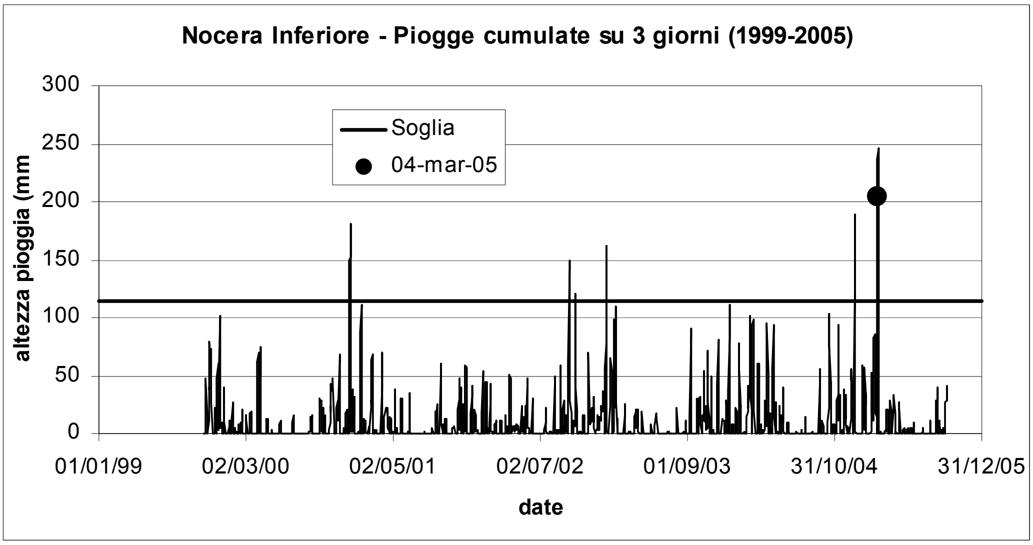

Figure 3.16. Rains cumulated over 1, 2 and 3 days from 1999 to 2005

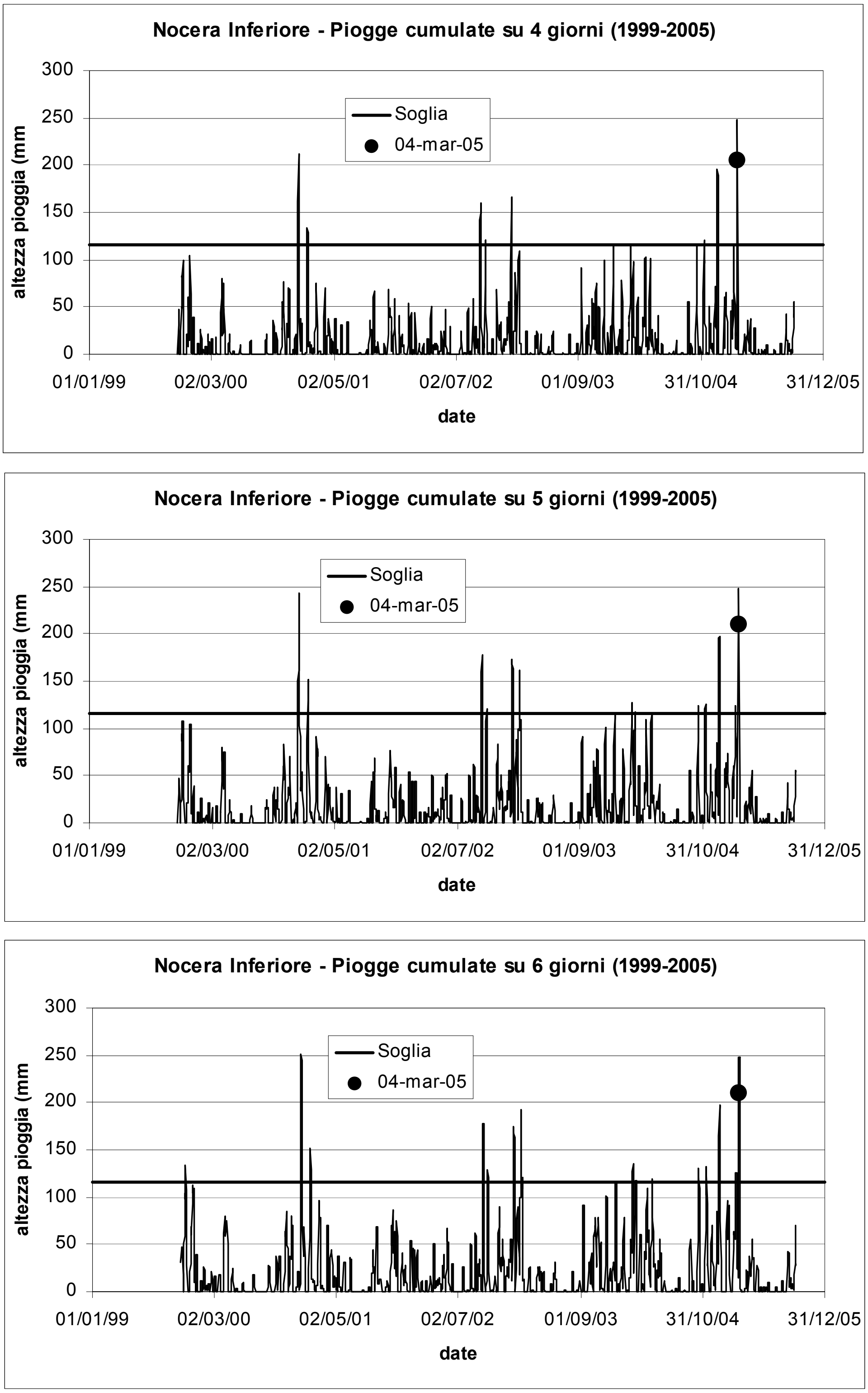

Figure 3.17. Rains cumulated over 4, 5 and 6 days from 1999 to 2005

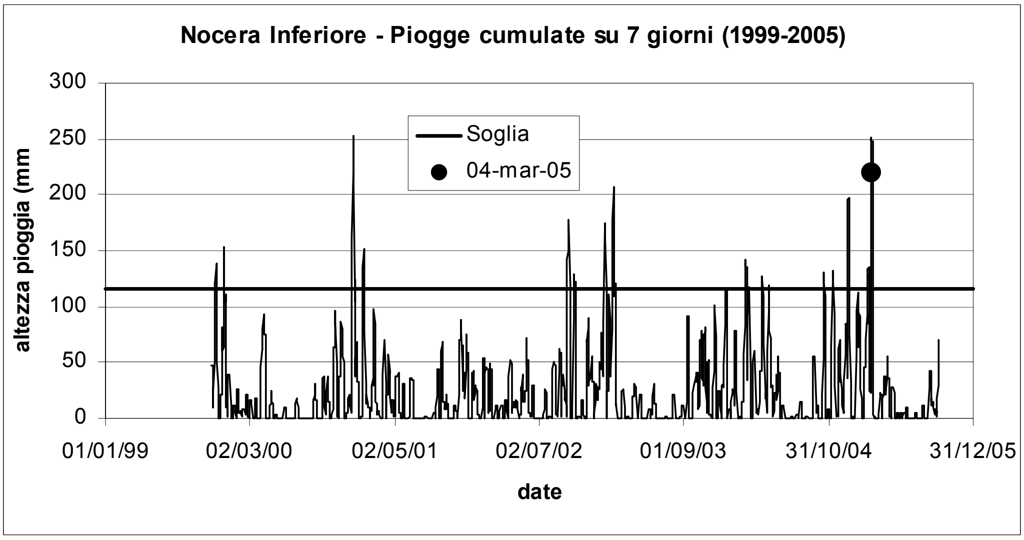

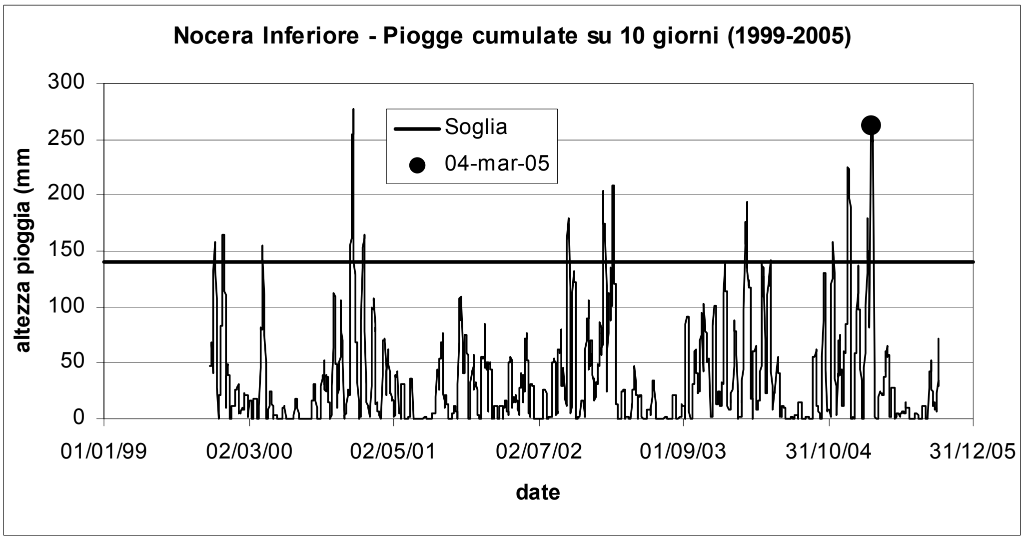

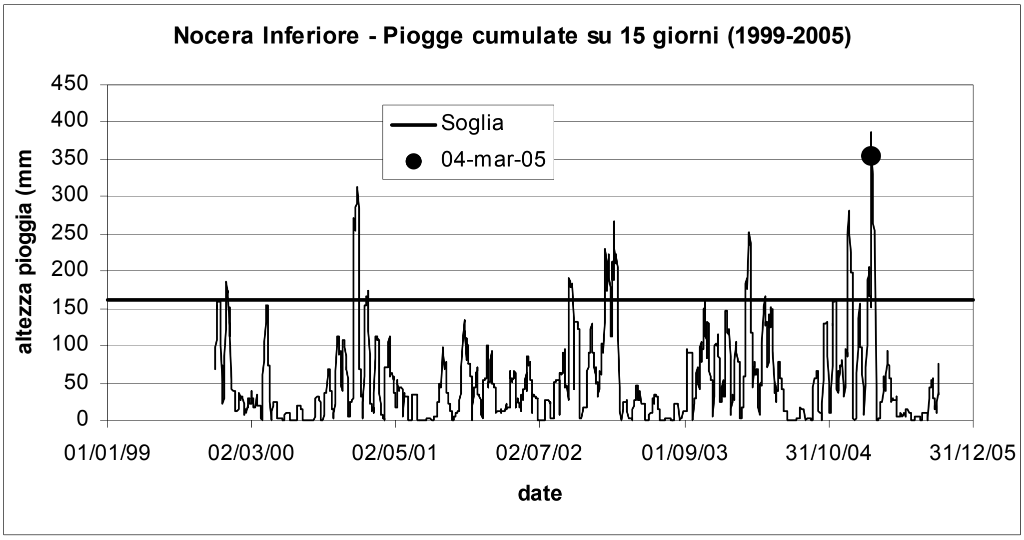

Figure 3.18. Rains cumulated over 7, 10 and 15 days from 1999 to 2005

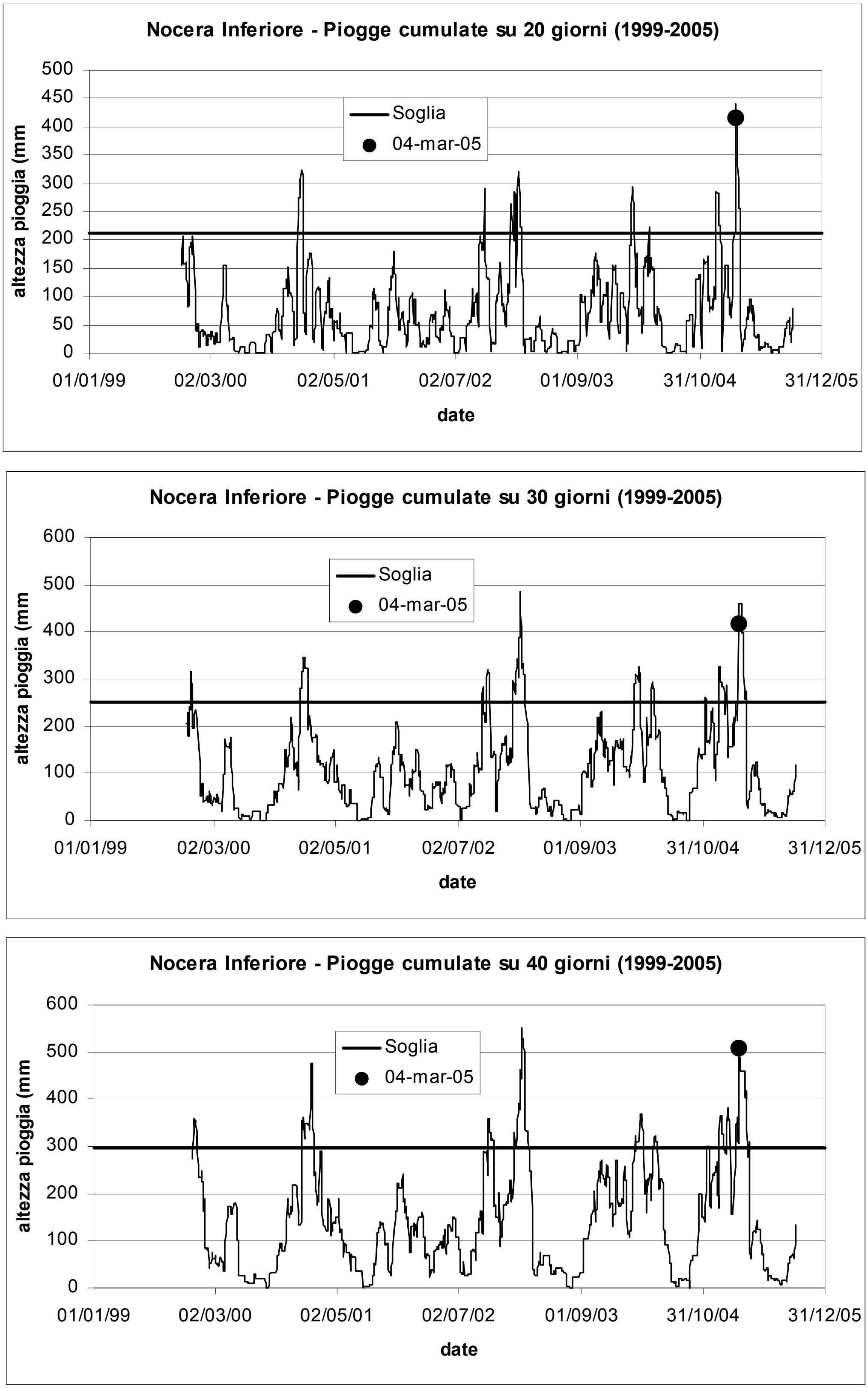

Figure 3.19. Rains cumulated over 20, 30 and 40 days from 1999 to 2005

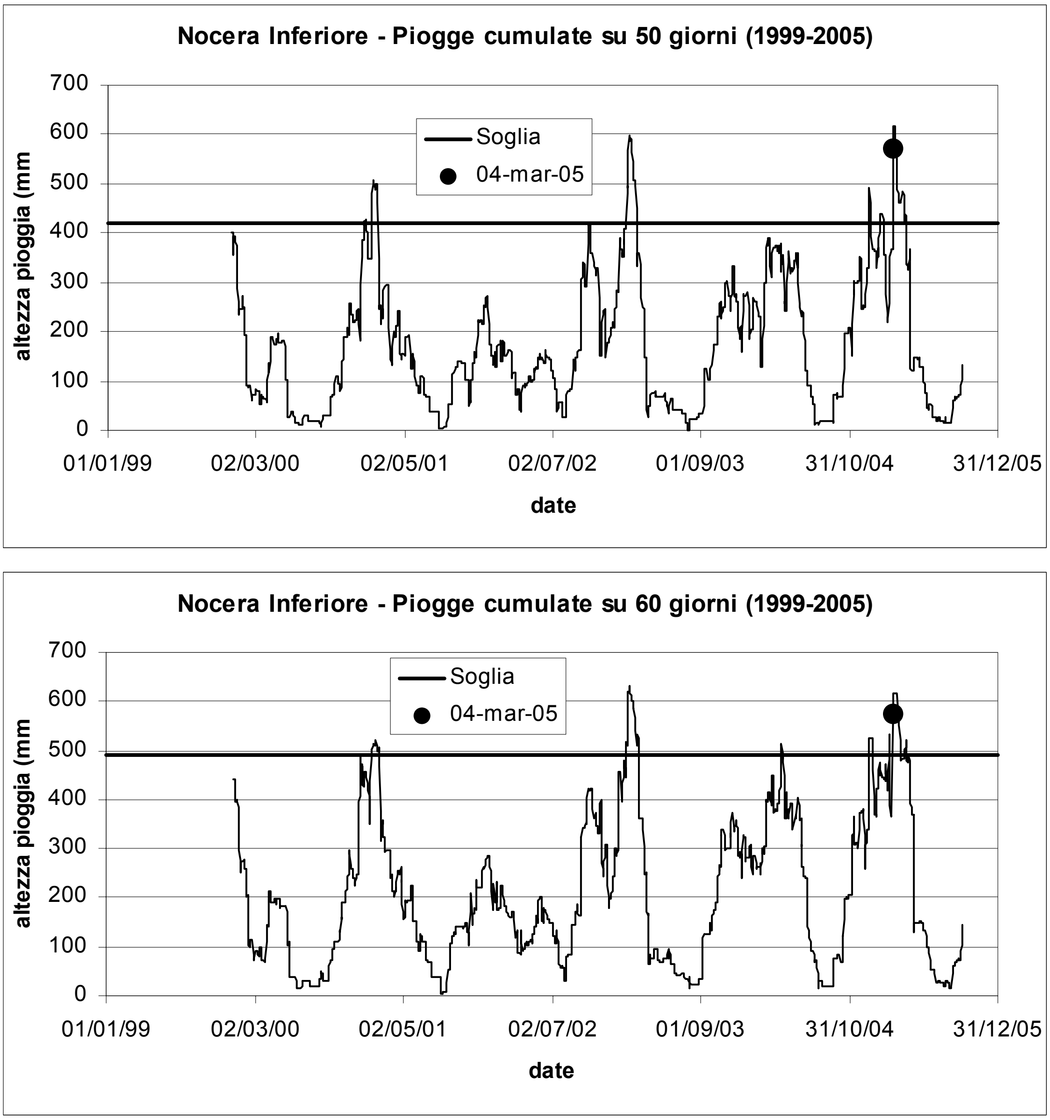

Figure 3.20. Rains cumulated over 50 and 60 days from 1999 to 2005

At the S. Pantaleone hill, a monitoring station of atmospheric and soil physical variables was installed (Figure 3.21 and 3.22). The monitoring station is located not far from the landslide site. The soils are very similar to those which outcrop in the landslide of March, 2005. The monitoring station was equipped with Jet-fill tensiometers installed at different depths. As well known, these instruments can measure soil suction up to 80 kPa, thus they may be reliably used in pyroclastic soils, since suction typically does not exceed 70 kPa.

Figure 3.21. Acquisition system of the monitoring station located on the S. Pantaleone hill

Figure 3.22. Tensiometers installed in pyroclastic soils of S. Pantaleone hill

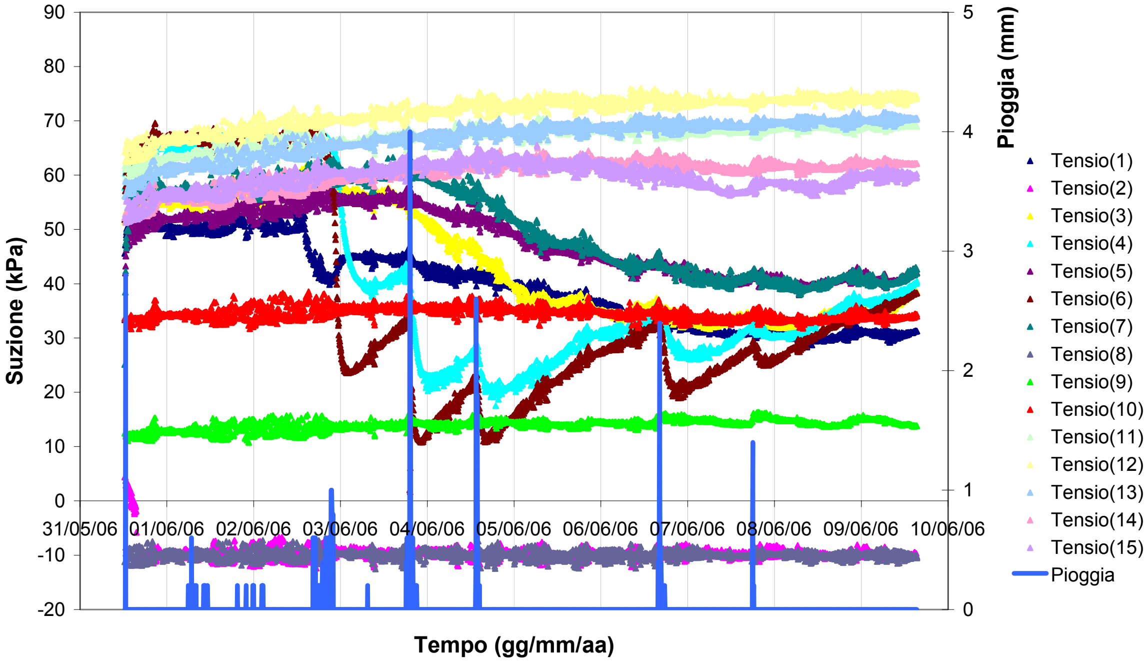

Figure 3.23. Measure of soil suction at S. Pantaleone hill

4. Conclusive remarks

This report contains information regarding the geomorphological setting, the monitoring records and the properties of soils about two Campanian sites, Camaldoli hill and Nocera Inferiore, where precipitation-induced landslides were triggered. The collected data may be considered functional to specific back-analyses of the events, which help to validate a model for landslide prediction.

The choice of the model depends on the scale of the problem. In particular, we believe that the most correct approach has to be based on a procedure that makes provision for the combined use of two differently scaled models: a *regional model* and a *local model*.
A *regional model* is typically GIS-based and enables to locate over wide areas as the timing as the location of potential landslides. This is allowed through slope stability calculations, performed by the use of a simple infiltration model, aimed to compute transient pore pressures changes caused by rainfall, coupled with a stability model for the evaluation of the factor of safety. The model subdivides the area into a grid formed by 3D-cells, which represent homogenous soil columns, each one of them characterized by own thickness, topographic parameters (derivable from a Digital Elevation Model of the area), mechanical and hydraulic properties, meteorological boundary conditions and initial hydraulic conditions. All data are generally saved to files, that can be imported by a GIS software for display or for further analyses.
It's worth noting that it's not easy to obtain detailed information for wide areas and frequently it is even impossible to collect the complete input data. Due to this aspect, a

regional model has to be thought useful essentially to individuate over broad areas those slopes which are more susceptible to failure and which therefore need more detailed analyses. These last can be performed by a *local model*, which is able to analyse the response of a single slope to rainfalls, using a more sophisticated approach which allows to contemporarily resolve not only hydraulic problems (e.g. infiltration, pore pressure regime) and mechanical problems (e.g. stability, displacements range), but also thermodynamic problems (e.g. heat flux, evapotranspiration). In particular, the analysis with a *local model* is characterized by a detailed evaluation, in correspondence of each calculation node, of a factor of safety corresponding to the ratio of the resisting shear stress and the driving shear stress. It's evident that in order to fully exploit its potentiality, a *local model* need a more detailed knowledge of each input parameter.

Next technical reports will provide some practical examples of both the models applied to the test cases of Camaldoli hill and of Nocera Inferiore.

5. References

Anderson CE and Stormont JC (2006). Changes in the soil moisture characteristics due to porosity variation. Unsaturated Soils 2006, Geotechnical Special Publication No. 147. Vol.2, pp. 1360-1370

Baum RL, Savage WZ and Godt JW (2002). TRIGRS—A fortran program for transient rainfall infiltration and grid-based regional slope-stability analysis. U.S. Geological Survey Open-File Report 02-0424

Brooks RH and Corey AT (1964). Hydraulic properties of porous media. Hydrology Paper No.3, Colorado State Univ., Fort Collins, Colorado

Calcaterra D, de Riso R, Evangelista A, Nicotera MV, Santo A and Scotto Di Santolo A (2003). Slope instabilities in the pyroclastic deposits of the carbonate Apennine and the Phlegraean district (Campania, Italy). Proc. Int. Workshop "Occurrence and Mechanisms of Flow-like Landslides in Natural Slopes and Earthfills", Sorrento, May 14–16, 2003, pp. 61–76.

Croce A and Pellegrino A (1967). Il sottosuolo di Napoli. Caratterizzazione geotecnica del territorio urbano. Proc. VIII Convegno di Geotecnica, Cagliari, vol. 3.

Di Crescenzo G, Rotella M and Santo A (2007). Il contributo della geologia per lo studio dei meccanismi di innesco di colate rapide di fango al campo sperimentale di Monteforte Irpino (primi risultati). In Piattaforme Evolute di Telecomunicazioni e di Information Technology per l'Offerta di Servizi al settore Ambiente PETIT-OSA a cura di C.Nunziata Aracne editrice srl Roma ISBN 978-88-548-1184-3.

Evangelista A and Scotto di Santolo A (2001). Mechanical behaviour of unsaturated pyroclastic soil. Proc. Int. Conf. Landslides: Causes, Impacts and Countermeasures, Davos, pp. 35-44

Haines WB (1930). Studies in the physical properties of soil. J. Agric. Sci. 20, pp. 97–116

Hilf JW (1956). An investigation of pre-water pressure in compacted cohesive soils. Ph.D. dissertation, Tech. Memo. No.654, U.S. Dep. of the Interior, Bureau of Reclamation, Design and Construction Div., Denver

Ho KMY, Ng CWW, Ho KK S and Tang WH (2006). State-dependent soil-water characteristic curves (SDSWCCs) of weathered soils. Unsaturated Soils 2006, Geotechnical Special Publication No. 147. Vol. 2, pp. 1302-1313

Iverson RM (2000). Landslide triggering by rain infiltration. Water Resour Res, 36, pp. 1897–1910

Jenson SK and Domingue JO (1988). Extracting Topographic Structure from Digital Elevation Data for Geographic Information Systems Analysis. Photogrammetric Engineering and Remote Sensing 54(11), pp. 1593-1600.

Leong EC, Agus SS and Rahardjo H (2004). Volume change measurement of soil specimen in triaxial test. Geotechnical Testing Journal, Vol. 27, No. 1, pp. 1-10

Mitchell RJ and Mayer AS (1998). The significance of hysteresis in modeling solute transport in unsaturated porous media, J. Soil Sci. Soc of Amer. Vol. 62, No. 6, pp. 1506-1512

Mualem Y (1976). A new model for predicting the hydraulic conductivity of unsaturated porous media. Water Resources Research, 12, pp. 513-522.

Ng CWW, and Pang YW (2000). Experimental investigation of soil-water characteristics of a volcanic soil. Canadian Geotechnical Journal, Vol. 37, No. 6, pp. 1252-1264

Olivares L and Picarelli L (2003). Shallow flowslides triggered by intense rainfalls on natural slopes covered by loose unsaturated pyroclastic soils. Géotechnique, 53(2), pp. 283-288

Padilla JM Perera YY, Houston WN and Fredlund DG (2005). A new soil-water characteristic curve device. Proceedings of an international symposium on advanced experimental unsaturated soil mechanics EXPERUS 2005. Trento, Italia, June 27-29, 2005, pp. 15-22

Pham HQ, Fredlund DG, and Barbour SL (2005). A study of hysteresis models for soil-water characteristic curves. Canadian Geotechnical Journal, Vol. 42, pp. 1548-1568

Picarelli L, Evangelista A, Rolandi G, Paone A, Nicotera MV, Olivares L, Scotto di Santolo A, Lampitiello S and Rolandi M (2006). Mechanical properties of pyroclastic soils in Campania Region. Proceedings of the Second International Workshop on Characterisation and Engineering Properties of Natural Soils, Singapore

Picarelli L., Santo A., Di Crescenzo G., Olivares L. (2008). Macro-zoning of areas susceptible to flowslide in pyroclastic soils in Campania Region. Proc. 10° Int. Symp. on Landslides, Xi'an, in corso di stampa

Rampino C, Mancuso C, and Vinale F (1999). Laboratory testing on an unsaturated soil: equipment, procedures and first experimental results. Can. Geotech. J. 36, pp. 1-12

Rojas JC, Zingariello MC, Mancuso C, Vinale F (2006). Un apparecchio per prove di ritenzione idrica a suzione e carico controllati. Incontro Annuale dei Ricercatori di Geotecnica 2006. June 26-28, Pisa, Italy

Romero E and Vaunat J (2000). Retention curves in deformable clays. Experimental evidence and theoretical approaches in unsaturated soils, pp. 91-106

Savage WZ, Godt JW and Baum RL (2003). A model for spatially and temporally distributed shallow landslide initiation by rainfall infiltration. Proc. III Int. Conf. on Debris flow hazards mitigation: mechanics, prediction, and assessment, Davos, Switzerland, pp 179–187

Sheeran DE and Krizek R (1971). Preparation of homogeneous soil samples by slurry consolidation. Journal of Materials, ASTM, Vol. 6, No. 2, pp. 356-373

van Genuchten MTh (1980). A closed-form equation for predicting the hydraulic conductivity of unsaturated soils. Soil Sci. Soc. Am. J. 44, pp. 892-898

Vanapalli SK, Fredlund DG, Pufahl DE and Clifton AW (1996). Model for the prediction of shear strength with respect to soil suction. Canadian Geotechnical Journal, 33, pp. 379-392

Vanapalli SK, Fredlund DG and Pufahl DE (1999). The influence of soil structure and stress history on the soil-water characteristics of a compacted till. Geotechnique 49, No.2, pp. 143-159

Vereecken H, Diels J, and Viaene P (1995). The effect of soil heterogeneity and hysteresis on solute transport: a numerical experiment. Ecological Modelling Journal 77, pp. 273-288

Wang X and Benson CH (2004). Leak-free pressure plate extractor for measuring the soil water characteristic curve. Geotechnical Testing Journal, Vol. 27, No. 2, pp. 1-10

Wissa AEZ and Heiberg (1969). A new one-dimensional consolidation test. MIT research report 69-9